

**FRIEDRICH ALEXANDER UNIVERSITÄT
ERLANGEN-NÜRNBERG**

Simulation based optimization of granular damping devices

by

Mohammad Hassan Nadjafabadi Farahani

A thesis submitted in partial fulfillment for the degree of
Master of Science

in the
Faculty of Engineering
Institute for Multiscale Simulation

July 2015

Declaration of Authorship

I, Mohammad Hassan Nadjafabadi Farahani, declare that this thesis titled, ‘Simulation based optimization of granular damping devices’ and the work presented in it is done by myself and have not used sources or means without declaration in the text. Any thoughts or quotations which were inferred from these sources are clearly marked as such. This thesis was not submitted in same or in a substantially similar version, not even partially, to any other authority to achieve an academic grading and was not published elsewhere.

Signed:

Acknowledgements

Foremost, I would like to express my very great appreciation to Prof. Thorsten Pöschel for allowing me to work in his group and his valuable advice.

Furthermore, I would also like to offer my special thanks to Dr. Patric Müller. I am extremely thankful and indebted to him for his remarks, comments and in particular for spending very much time to instruct me how to write this thesis.

I also would like to thank Dr. Eric Partelli and Jonathan Kollmer for their useful comments and discussions.

I take this opportunity to express gratitude to all of the members of the institute of multiscale simulation for their help and support.

Contents

Declaration of Authorship	i
Abstract	ii
Acknowledgements	iii
1 Introduction	1
2 Simulation Method	8
2.1 Molecular Dynamics	8
2.2 Force model	8
2.3 Velocity Verlet Algorithm	14
2.4 Time step	15
2.5 Contact detection	15
2.6 Software	16
3 Simulation and Results	18
3.1 Effect of vibration properties	18
3.1.1 Amplitude	18
3.1.2 Frequency	21
3.2 Influence of material properties	22
3.2.1 Poisson ratio and Young's modulus	22
3.2.2 Coefficient of friction	25
3.2.3 Coefficient of restitution	28
3.3 Filling ratio	30
4 Optimization	34
4.1 Multicomponent damper	34
4.2 Complex cavity geometry	40
5 Conclusion	45
A LIGGGHTS Sample Script	47

B LIGGGHTS commands	49
B.1 LIGGGHTS	49
B.1.1 initialization	49
B.1.2 Atom definition	50
B.1.3 Settings	50
B.1.4 Run a simulation	52
C LIGGGHTS bug	53
Bibliography	54

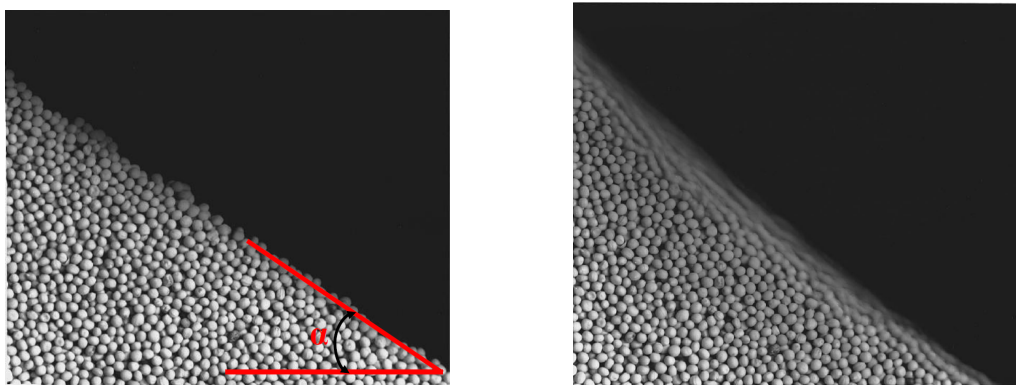
Dedicated to my parents

Chapter 1

Introduction

Granular materials consist of discrete macroscopic particles. The force between them is repulsive in absence of cohesion between particles and long range attractive forces such as gravity play no role [1].

Granular materials cannot be classified as solid, liquid, or gas, because of their unusual phase of matter. For instance, consider a pile of sand at rest with a surface slope lower than angle of repose (α) as in figure 1.1(A). These sand particles behave like solid. The material remains at rest even though gravitational forces create macroscopic stresses on its surface. With the slope getting larger than the angle of repose, sand particles start flowing as in figure 1.1(B). The sand pile cannot be considered as fluid, since the flow only exists in the boundary layer at the pile's surface without movement in the bulk [2].



(A) A pile of mustard seeds with the surface angle less than angle of repose (α) [2]. (B) The same pile after the slope has been increased slightly to create an avalanche[2].

FIGURE 1.1: Different behavior of a pile of mustard seeds when the surface slope changes.

Granular materials have some features. For instance, one may assume granular flow as a dense gas, because gases are made of discrete particles with negligible cohesive forces

between them. However, the thermal energy, $K_B T$, is insignificant in granular materials for ordinary temperature. Take typical sand as an example. Its potential energy, mgd , where m and d are the mass and diameter of grain and g is the Earth's gravity, is at least 10^{12} times $K_B T$ at room temperature. The other important feature of granular materials is that the interaction between grains is dissipate [1]. In the microscopic objects like atoms, the collisions are elastic and the kinetic energy is conserved; while in the macroscopic objects, the collision is inelastic and the kinetic energy is not conserved. Some reasons are that the collision may deform the shape of objects and also there is a friction between the objects' surfaces.

The dissipative properties of granular materials make them interesting be used as a damper. A Granular damper is a device used to attenuate the oscillation of a vibrating structure or machinery.

Two typical forms of a granular damper are the box-base [3] and the piston-base [4]. The box-base is a container or cavity that is partly filled by granular particles which may be attached to a vibrating machinery to diminish the oscillations as in figure 1.2(A). The piston-base is a piston that may be attached to vibrating machinery and is inserted into a bed of granular materials [5] like figure 1.2(B). We investigate the box-base granular damper in our work.

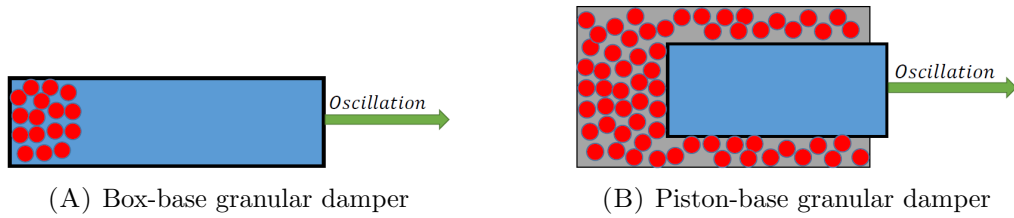


FIGURE 1.2: Different types of granular damper

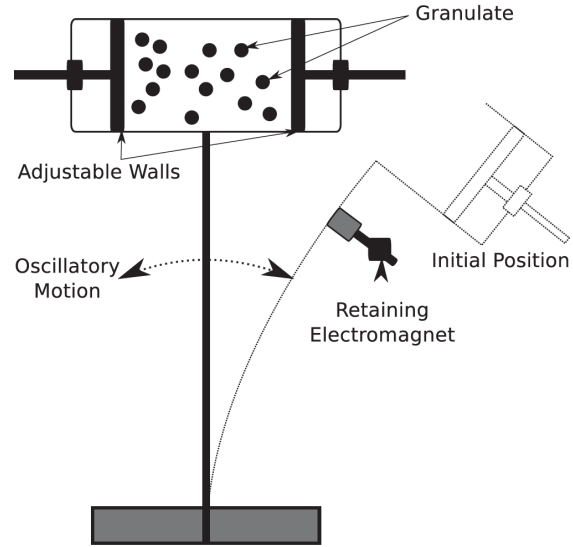
Granular dampers have some advantages which make them attractive to technical applications. They are simple devices which consist of particles enclosed in a container. They are useful in portable equipment and space applications since they do not require an anchor unlike conventional dampers which need an anchor to restrict the motion of the system [6]. They also resist to aging compared to the oil and rubber component of traditional dampers [6]. They can work in a wide range of temperatures while the viscous dampers are more sensitive to temperature gradient [6]. These specifications make them easy to maintain [6]. Granular dampers cover a wide range of applications such as vibration attenuation in medical tools [7], metal cutting [8], sport equipment [9], bonding machines [10], brake drum [11] and structural damping [12].

One of the effective parameters on the behavior of granular material is gravity. *Saluña et.al* [13] by means of numerical simulation, show how the gravity can affect the energy dissipation regimes. They vibrate a container of granular materials horizontally with

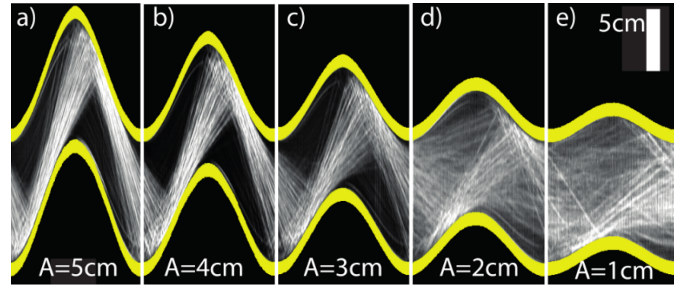
sinusoidal motion, $x(t) = A\sin(\omega t)$, where A and ω are amplitude and frequency of vibration. Their results show three different energy dissipation regimes or phases in the amplitude-frequency plane of the external forcing. These regimes are solid, convective and gaslike phases. Transition between these regimes happens when the effective acceleration $\Gamma = A\omega^2/g$ and amplitude of the velocity of vibration, $A\omega$, change. They have shown that the transition point is $\Gamma = 1$.

An efficient operation of granular damper is expected when the average kinetic energy of the particles is larger than their average potential energy [6] which motivated others like [6] and [14] to perform experiments to investigate the energy dissipation of granular dampers under weightless conditions.

Kollmer et.al [15] have conducted an experiment where a granular damper is attached to an oscillating spring as in figure 1.3(A). They have shown that two different dynamical states of the granulate exist.



(A) A granular damper attached to an oscillating spring [6].



(B) Modes of excitation of the granulate in a vibrating container. Each subfigure shows the granulate moving in a box sinusoidally driven at constant amplitude A . The position of the container is highlighted in color. The figure is taken from article [15].

FIGURE 1.3: A granular damper attached to an oscillating spring and its mode of excitation.

In figure 1.3(B) they show the dynamic state of granulate in a box attached to an oscillating spring. For large amplitude, similar to figure 1.3(B)(a)-(c), particles move as a cluster and arrive when the velocity of the wall changes and moves in the opposite direction of the granulate cluster. Therefore, the particles arriving at the incoming wall are collected and accumulated as a dense packed layer at the container's wall. Then, when the container decelerates, the cluster of particles leaves the wall and it moves towards the opposite wall [15]. When they impact the opposite wall, a large part of the energy is dissipated because of inelastic collisions. This behavior was called collect-and-collide regime [6]. In this regime, the center of mass of granulate oscillates relative to the center of box [see figure 1.4(B)]. Both the experimental and the theoretical aspects of the collect-and-collide regime, were investigated in [6]. For small amplitude, similar to figure 1.3(B)(d)-(e), the granulate behaves like a gas and occupies the entire volume of the container[15]. In other words, the center of mass of the granulate is almost in the center of the box [see figure 1.4(A)].

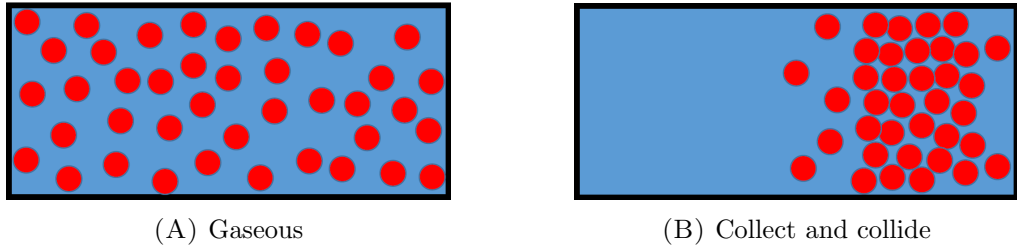


FIGURE 1.4: Different behavior of the dynamical state of granulate with different amplitude of oscillation.

In particular we focus on the experiment done by *Sack et.al* [14]. They filled a container partly by granular particles and applied a sinusoidal oscillations of adjustable angular velocity and amplitude during a parabolic flight to have a weightless condition. The main difference between their experiment and the previous one is that they put the container under permanent harmonic vibration which leads to steady-state vibration. The energy dissipates through particle-particle and particle-wall interactions. These interactions show their effects on the forces that particles induced on the container's walls. Therefore, they calculated the dissipation in one period of oscillation, $T \equiv 2\pi/\omega$, with the following formula:

$$E_{diss} = \int_T \dot{x}(t)f(t)dt \quad (1.1)$$

Where \dot{x} is the velocity of the container's wall which has a sinusoidal motion $x(t) = A \sin(\omega t)$. $f(t)$ is the impact force between the particles and the wall. They show that

the major force to the wall is the one which is perpendicular to the direction of vibration. Since the granulates move as a cluster in the collect-and-collide regime, they suggest a one-particle model for granular dampers in this regime. In this model, there is a single-quasi particle, cycling in the container. When it collides to the wall, it loses all its relative velocity with respect to the wall. The energy dissipation of this quasi-particle in one stroke (half period) is :

$$E_{diss} = \frac{1}{2}m(v - v_{wall})^2 \quad (1.2)$$

Where m and v are the mass and velocity of the quasi-particle respectively and v_{wall} is the velocity of the wall at the time of collision. At the time $t = 0$ acceleration vanishes and the wall has the maximum velocity $v_{wall} = A\omega$. This velocity of the quasi-particle is conserved until the next impact to the opposite wall. Since the maximum velocity of the wall is $A\omega$, the maximum relative velocity is $2A\omega$ [16]. Therefore, the maximum energy dissipation per half-period is :

$$E_{diss}^{max} = 2mA^2\omega^2$$

With this equation, equation 1.2, and considering that the particle velocity after time $t = 0$ when the particle leaves the wall is $A\omega$, the dissipation energy in the collect-and-collide regime can be written as:

$$E_{diss} = \frac{1}{2}m[A\omega - A\omega\cos(\omega t_c)]^2 = \frac{1}{4}E_{diss}^{max}[1 - \cos(\omega t_c)]^2 \quad (1.3)$$

Where t_c is the time of collision of quasi-particle with the opposite wall. This time can be defined through the distance that the quasi-particle has traveled in the container.

$$v_{wall}t_c = A\omega t_c = A\sin(\omega t_c) + L_g \quad (1.4)$$

Where L_g is the gap length and is defined as the difference between box length and the thickness of the packed layer of particles [see figure 1.5].

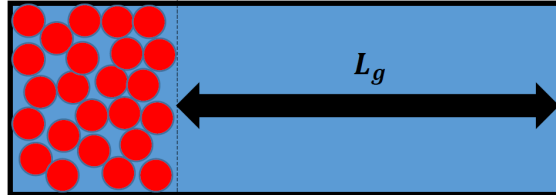


FIGURE 1.5: Front view to the container for showing the gap length

The condition $\omega t_c < \pi$ shows the collect-and-collide regime. Therefore, they used first order expansion around $\omega t_c = \pi$ in the Eq.1.4:

$$\omega t_c \approx \frac{\pi}{2} + \frac{L_g}{2A} \quad (1.5)$$

The result of the experiment of *Sack et.al* [14] is shown in the figure 1.6. It shows how the efficiency of damper ($\eta = \frac{E_{diss}}{E_{max}}$) changes with amplitude for different samples. For the amplitude $A < A_0$ we have gaseous regime and for amplitude $A > A_0$ we have collect-and-collide regime.

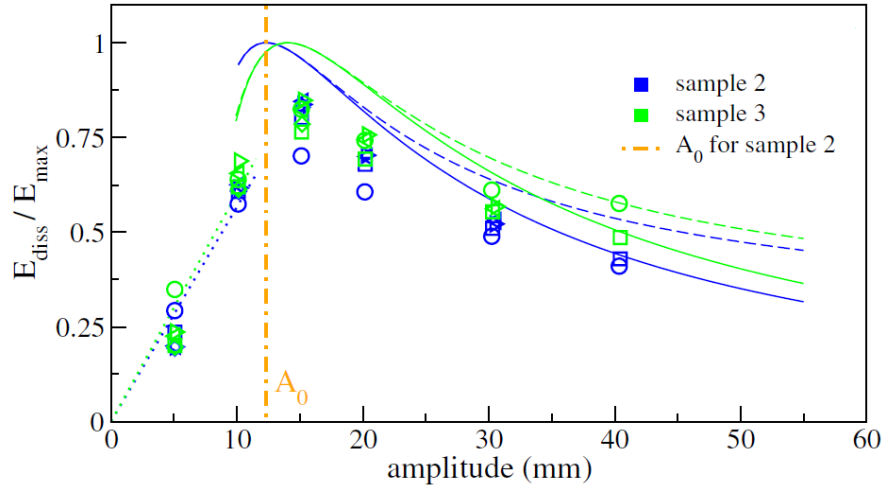


FIGURE 1.6: The efficiency-amplitude plot for different samples from article [14]

This threshold A_0 can be find when $\omega t_c = \pi$ in Eq.1.5:

$$A_0 = \frac{L_g}{\pi} \quad (1.6)$$

We can call this A_0 as an optimum amplitude, A^{opt} , since the maximum dissipation happens at this amplitude. This value can be useful in designing granular dampers.

In general, if we want to know the physics of a condensed matter system, we begin by studying its excitations [17]. These excitations are the vibrations in case of granular materials [17]. Typically, we have three types for vibration [5]. The first one is transient vibration [18] where vibrating device is put under an initial displacement or velocity. Then, the particles damp the resulting vibration. A Granular damper attached to oscillating spring has been investigated by *Kollmer et.al* [15] for this type of vibration. They give a quantitative explanation for initial linear decay and the residual amplitude when the linear decay stops. Figure 1.7 shows the attenuation of this spring damped by a granular damper. The other type of oscillation is the steady-state[19] vibration where the device is forced to have a driven vibration. This was in the work of *Sack et.al* [14]

which has been explained. The last type is stochastic vibration [20] where vibrations are random. In our study we concentrate on the steady-state vibration.

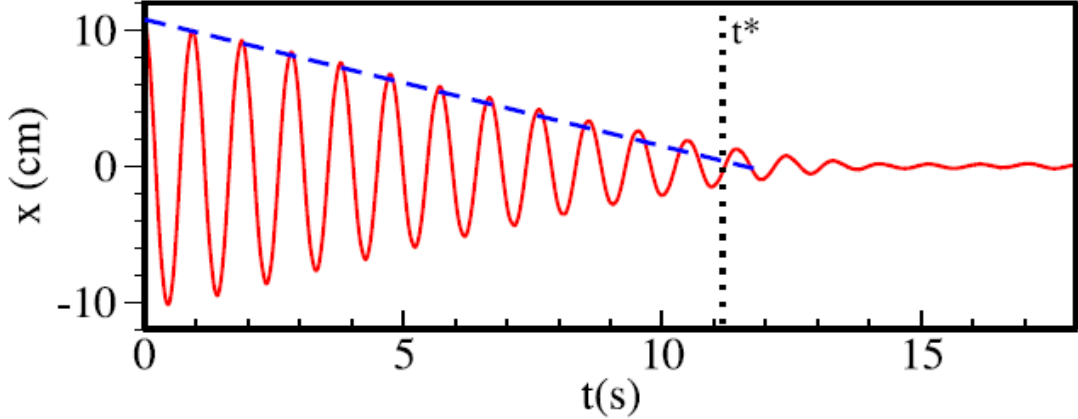


FIGURE 1.7: The Attenuation of a linear spring damped by a granular damper [15]

Conducting an experiment in weightless condition has some difficulties such as a requirement for parabolic flights. Therefore, the data is limited which motivates us to use a simulation. At first, we verify our simulation with existing experimental data. Then, we expand our simulation to extend data. For instance, we check the effect of material and vibration properties. At the end, we develop more versatile damping devices, for instance having a multi-unit granular damper, to cover a wider range of amplitudes with high efficient dissipation.

Chapter 2

Simulation Method

2.1 Molecular Dynamics

Granular materials are systems of macroscopic particles which interact with each other via mechanical contact and long-range force such as gravity are negligible in this contact. The governing equation which describes their motion is Newton's motion law [21]:

$$\frac{\partial \vec{r}_i}{\partial t^2} = \frac{1}{m_i} \vec{F}_i(\vec{r}_j, \vec{v}_j, \vec{\varphi}_j, \vec{\omega}_j) \quad (2.1)$$

$$\frac{\partial \vec{\varphi}_i}{\partial t^2} = \hat{j}_i^{-1} \vec{M}_i(\vec{r}_j, \vec{v}_j, \vec{\varphi}_j, \vec{\omega}_j) \quad (2.2)$$

where \vec{F}_i is the force and \vec{M}_i is the torque on particle i with mass m_i , tensorial moment of inertia \hat{j}_i , position \vec{r}_j , angular orientation $\vec{\varphi}_j$ and corresponding velocities \vec{v}_j and $\vec{\omega}_j$. One method to solve these equations is molecular dynamics. This is a numerical method that trajectories of all particles. In order to solve these equations, we need to know the contact force between particles which will be explained in next section.

2.2 Force model

In practice, the grains may have non-spherical shape, non-uniform materials and even compose of smaller grains. In following discussion we assume some simplification conditions. We consider that the particles are smooth, sphere and of uniform materials. The latter assumptions let us describe the particle deformation by continuum mechanics regardless of their molecular structure [22]. The *compression* between two particles i and

j is defined as:

$$\xi_{ij} = R_i + R_j - |\vec{x}_i - \vec{x}_j|$$

where R_i and R_j are the radii of two particles. The particles are in contact when $\xi_{ij} > 0$. Therefore, the force between the particles is:

$$\vec{F}_{ij} = \begin{cases} \vec{F}_{ij}^n + \vec{F}_{ij}^t & \xi_{ij} > 0 \\ 0 & \xi_{ij} \leq 0 \end{cases}$$

where $\vec{F}_{ij}^n, \vec{F}_{ij}^t$ are the forces in normal and tangential direction, respectively [21]. The normal force and tangential force cause changes in translational and rotational motion of particles, respectively. The normal unit vector points from the mass center of particle j to i :

$$\vec{n} = \frac{(\vec{x}_i - \vec{x}_j)}{|\vec{x}_i - \vec{x}_j|}$$

which has been shown in figure 2.1.

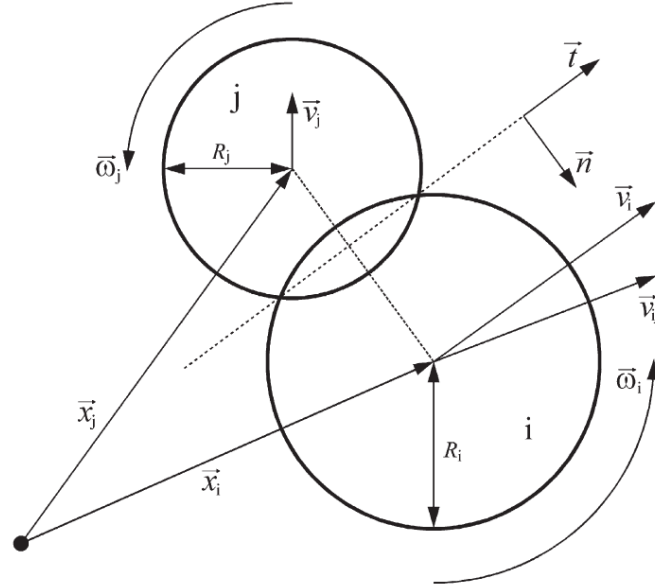


FIGURE 2.1: Contact of two spheres [23].

The relative velocity of particles surfaces at the point of contact in the tangential direction is

$$v_{rel}^t = (\vec{v}_j - \vec{v}_i) \cdot \vec{e}_t + R_i \omega_i + R_j \omega_j$$

where \vec{e}_{ij}^t is the tangential unit vector. If this velocity is equal to zero at the beginning of a contact, the impact is normal; otherwise, it is shearing or oblique [24]. The normal component of contact force is composed of two parts: elastic and viscous.

$$F^n = F_{elastic}^n + F_{viscous}^n$$

The elastic deformation means that after separation of contacting particles, they recover their initial shape [22]. We use the Hertz model to describe this force. For a single contact of two smooth sphere particles i and j with a maximum contact circle radius r_{max} , which is small compared to the particle diameter d_i and d_j , an elliptic pressure distribution $p(r)$ has been given by Hertz:

$$\left(\frac{p(r)}{p_{max}}\right)^2 = 1 - \left(\frac{r}{r_{max}}\right)^2$$

The maximum pressure is in the center of contact circle($r = 0$). The correlation between compression repulsive force, $F_{elastic}^n$, and pressure distribution:

$$F_{elastic}^n = 2\pi \int_0^{r_{max}} p(r) r dr = \frac{2}{3}\pi r_{max}^2 p_{max} \quad (2.3)$$

And the r_{max} is given by [25]:

$$r_{max} = \frac{\pi p_{max} R_{eff}}{2E_{eff}} \quad (2.4)$$

where the E_{eff} and R_{eff} are effective Young's Modulus and radius and defined as:

$$R_{eff} = \left(\frac{1}{R_i} + \frac{1}{R_j}\right)^{-1}, \quad E_{eff} = \left(\frac{1-\nu_i}{E_i} + \frac{1-\nu_j}{E_j}\right)^{-1}$$

where E is Young's modulus, ν is Poisson ratio of each particle. The compression, ξ , is [25]:

$$\xi = \frac{\pi p_{max} r_{max}}{2E_{eff}} \quad (2.5)$$

Using equations 2.5 and 2.4 in the equation 2.3:

$$F_{elastic}^n = k_n \xi^{3/2} \quad (2.6)$$

where $k_n = \frac{4}{3}\sqrt{R_{eff}}E_{eff}$.

The deformations change with time since the contacting particles move with respect to each other. Therefore, an additional dissipation force arises in the opposite direction to

the relative particle motion. Thus, these dissipative processes cause a viscous contribution to the stress tensor [22]. *Brilliantov et.al* [26] have shown a relation between the elastic and dissipative stress tensors which finally leads to the total dissipative force:

$$F_{dissipative}^n = A \dot{\xi} \frac{\partial}{\partial \xi} F_{elastic}^n(\xi) \quad (2.7)$$

where A is a dissipative constant and as a function of viscous and elastic material constants:

$$A = \frac{1}{3} \frac{(3\eta_j - \eta_i)^2}{(3\eta_j + 2\eta_i)} \left[\frac{(1 - \nu^2)(1 - 2\nu)}{E\nu^2} \right]$$

which $\eta_{i,j}$ is viscous material constant that relates the dissipative stress tensor to the deformation rate tensor. The total normal force considering equations 2.7 and 2.6 [21]:

$$F^n = k_n \xi^{3/2} + \gamma_n \sqrt{\xi} \dot{\xi} \quad (2.8)$$

$$\text{where } \gamma_n = \frac{3}{2} k_n \frac{A_i + A_j}{2}.$$

The problem here is that the dissipative constant A is not directly available. *Schwager et.al* [27] have shown a relationship between this constant and the coefficient of restitution in nonadhesive viscoelastic sphere. The coefficient of restitution relates to the deformation rate before and after collision:

$$\epsilon = -\frac{\dot{\xi}(t_c)}{\dot{\xi}(0)} = -\frac{\dot{\xi}(t_c)}{v}$$

where t_c is the duration of the collision. To find this relation first consider the Newton's equation of motion for the collision of viscoelastic sphere:

$$\ddot{\xi} + \frac{k_n}{m_{eff}} \xi^{3/2} + \frac{\gamma_n}{m_{eff}} \sqrt{\xi} \dot{\xi} = 0 \quad (2.9)$$

where $m_{eff} = (\frac{1}{m_i} + \frac{1}{m_j})^{-1}$. The initial conditions:

$$\xi(0) = 0, \dot{\xi} = v$$

Equation 2.9 contains parameters k, γ_n, m_{eff} and v with two scales of time and length. An appropriate choice of scales can be reduce the number of free parameters to one. *Schwager et.al* [27] have used a series expansion of the direct collision for the first part of the collision and a series expansion of the time-inversed collision for the second part. Therefore, they use velocity-independent length scale $\xi = k^{-2/5}$. Thus, the time and

length scale read:

$$\xi = \frac{x}{k^{2/5}} , \quad t = \frac{\tau}{k^{2/5} v^{1/5}}$$

and the Eq.2.9 becomes:

$$\begin{aligned} \ddot{x} + \alpha v^{-1/5} \dot{x} \sqrt{x} + v^{-2/5} x^{3/2} &= 0 \\ x(0) = 0 , \quad \dot{x}(0) &= v^{4/5} \end{aligned}$$

where $\alpha = \gamma_n k_n^{-3/5} m_{eff}^{2/5}$. They have used trajectory of particles during the collision with a series of half-integer powers of τ ($\sqrt{\tau}$), to solve these equations. After a complicated mathematical process, they have shown the exact solution for the coefficient of restitution:

$$\epsilon = 1 + \sum_{k=0}^{\infty} h_k \left(\underbrace{\beta^{1/2} v^{1/10}}_{v_*} \right)^k = 1 + \sum_{k=0}^{\infty} h_k v_*^k \quad (2.10)$$

where β is:

$$\beta = \frac{3}{2} A \left(\frac{k_n}{m_{eff}} \right)^{2/5}$$

with the condition:

$$F(t_c) = 0 \quad \text{with} \quad t_c > 0$$

which defines the end of collision to prevent attractive force. The condition $\xi(t_c) = 0$ may lead to $F(\xi, \dot{\xi}) < 0$ which violates the strict repulsive force between colliding grains in the absence of adhesion. This means that the collision may be completed even before $\xi = 0$. Therefore, the particles' surface loses contact slightly even with $\xi > 0$. As a consequence, the particles gradually recover their spherical shape after they lose contact. This behavior is called delayed recovery of the particles in the study of *Schwager et.al* [27].

The Eq.2.10 is a universal equation since the coefficient β covers the material and particle properties and the h_k are pure numbers which are independent of the material and particle properties.

The Eq.2.10 has two problems. First, it converges slowly. For instance, we need 20 terms of the series expansion to have quadratic order of v for finding ϵ . Second problem is that the truncate the series diverges to $\epsilon \rightarrow \pm\infty$ depending on the sign of h_k [28]. To solve these problems, *Müller et.al* [28] use a Padé approximation.

The Padé approximant is a rational function of two power series to approximate a given

function. For instance, consider a function $f(v_*)$ and a rational function:

$$R(v_*) = \frac{p(v_*)}{q(v_*)}, \quad p(v_*) = \sum_{i=0}^m a_i v_*^i, \quad q(v_*) = \sum_{i=0}^n b_i v_*^i$$

The rational function $R(v_*)$ is also shown as $[m/n]_f(v_*)$, is called Padé approximant to function $f(v_*)$. Consider $f(v_*)$ as a series, then:

$$f(v_*) - R(v_*) = O(v_*^{m+n+1})$$

Using $[1/4]_\epsilon(v_*)$ for function $\epsilon(v_*)$ in Eq.2.10, has been shown in the study of Müller *et.al* [28] that is in good agreement with the exact solution. The relative coefficient which they used is in table 2.1.

m	n	a_i	b_i
1	4	$a_0 = 1.0$	$b_0 = 1.0$
		$a_1 = 0.501086$	$b_1 = 0.501086$
		$b_2 = 1.15345, b_3 = 0.577977, b_4 = 0.532178$	

TABLE 2.1: Coefficient of Padé approximat for Eq.2.10 in [28].

The other component of contact force is in the tangential direction of collision. Generally, this force is connected to the normal force by the Coulomb laws of friction:

$$F^t \begin{cases} \leq \mu_s F^n & \text{for static friction } (v_{rel}^t = 0) \\ = \mu_d F^n & \text{for dynamic friction } (v_{rel}^t \neq 0) \end{cases} \quad (2.11)$$

where μ_s and μ_d are the coefficient of static and dynamic frictions, respectively. Normally, $\mu_s > \mu_d$ but we can consider them almost with same value in most applications [24]. In the case of static friction the \vec{F}^t compensates the external unknown force \vec{F}_{ext}^t applied to the contact, so that $v_{rel}^t = 0$ is conserved. When $\vec{F}_{ext}^t > \mu_s F^n$, one enters to the dynamic friction regime in Eq.2.11. One expects the condition for dynamic friction to be satisfied since strains are small and therefore the normal stress is small. While, in the central regions the static friction may happen because of large strains and stresses there. This leads to the development of annulus of microslip surrounding an inner region of sticking in the contact area [24]. The size and the form of the annulus of microslip depend on the loading-unloading history of the contact [24]. Mindlin has discussed the tangential friction forces between two elastic spheres for the case of several loading-unloading histories and assuming the Hertz theory to hold [24]. This model for the elastic part of tangential force is [29]:

$$F_{ela}^t = \int_{path} k_t \sqrt{R_{eff} \xi} ds$$

where:

$$k_t = \left[\left(\frac{4E_i}{(2 - \nu_i)(1 + \nu_i)} \right)^{-1} + \left(\frac{4E_j}{(2 - \nu_j)(1 + \nu_j)} \right)^{-1} \right]^{-1}$$

Several references [30, 31] suggest considering the dissipative part similar to dissipative part of normal force:

$$F_{diss}^t = A_t \sqrt{R_{eff}} \xi v_{rel}^t \quad (2.12)$$

The tangential dissipative parameter, A_t , characterizes the surface roughness. It is chosen such that the prefactors of the normal and tangential deformation rates ($\dot{\xi}$ and v_{rel}^t) in the Eq.2.8 and Eq.2.12, respectively, are of the same order of magnitude [31]. Using this assumption in Ref.[32] found a good agreement between simulation results and experimental values. Comparison of Eq.2.8 and Eq.2.12, give $A_t = AE_{eff}$ [31]. In summary, the magnitude of tangential force is:

$$F^t = \min(F_{ela}^t + F_{diss}^t, \mu F^n) \quad (2.13)$$

2.3 Velocity Verlet Algorithm

The concept of discretization in numerical mathematics explains the transition from a problem that is posed on a continues interval to a problem that is only posed at a finite number of points [33]. Discretization is used in the solution of differential equations to transform the differential equations into a system of equations with an approximate solution only at the chosen points [33]. One of the efficient and at the same time stable approaches for the time discretization of Newton's equations (Eq.2.1 and 2.2) is the Verlet algorithm [33]. One of the variants of Verlet algorithm is velocity Verlet algorithm. In this method, the position and velocity update at the same value of the time variable.

- $\vec{x}(t + \Delta t) = \vec{x}(t) + \vec{v}(t)\Delta t + \frac{1}{2}\vec{a}(t)\Delta t^2 + O(\Delta t^4)$
- $\vec{v}(t + \Delta t) = \vec{v}(t) + \frac{1}{2}[\vec{a}(t) + \vec{a}(t + \Delta t)]\Delta t + O(\Delta t^2)$

where Δt is the time step and \vec{a} is the acceleration of the particle. The local errors for position and velocity are $O(\Delta t^4)$ and $O(\Delta t^2)$. However, the global error is $O(\Delta t^2)$ for both velocity and position.

The implementation scheme for this algorithm is [34]:

1. Calculate: $\vec{v}(t + \frac{\Delta t}{2}) = \vec{v}(t) + \frac{1}{2}\vec{a}(t)\Delta t$
2. Calculate: $\vec{x}(t + \Delta t) = \vec{x}(t) + \vec{v}(t + \frac{\Delta t}{2})\Delta t$
3. Derive $\vec{a}(t + \Delta t)$ from the interaction
4. Calculate: $\vec{v}(t + \Delta t) = \vec{v}(t + \frac{\Delta t}{2}) + \frac{1}{2}\vec{a}(t + \Delta t)\Delta t$

2.4 Time step

In order to solve the velocity Verlet scheme we need to know how large our time step can be. The most important time is the duration of contacts between two particles. In reference [35] the contact duration for impact of two elastic spheres is given:

$$\tau = 3.218R \left(\frac{\sqrt{2}\pi\rho(1-\nu^2)}{E} \right)^{\frac{2}{5}} (-\dot{r})^{\frac{1}{5}}$$

where ρ is density and \dot{r} is the maximum relative velocity .

We need to divide this number to some arbitrary factor to ensure the satisfactory of numerical accuracy [24]. We choose time step so that:

$$\Delta t \leq \frac{\tau}{100}$$

2.5 Contact detection

The performance bottleneck of Molecular Dynamics simulations is the force computation [21]. It is completely inefficient to check each pair of particles for possible contacts which is $O(N^2)$ where N is the number of particles. Since the forces between granulates are of short range, the force computation can be restricted to pairs of particles which are close neighbors [21]. Therefore, we can have a list of potential contacts periodically which this list is the idea of Verlet list or neighbor list [30]. For each particle, there is the Verlet list which records all of close neighbors for this particle [21]. The evaluation of actual contacts is based on this list at each time step. This allows us to exclude pairs of particles that are too far away from each other [30]. A pair of spherical particles is included in the neighbor list if

$$|\vec{x}_i - \vec{x}_j| < R_i + R_j + s$$

where s is the so-called Verlet or skin parameter that can be chosen freely within some bounds [30]. This parameter shows how long the list will stay valid. The list is valid for

$$N_{verlet} = \frac{s}{2v_{max}\Delta t}$$

where v_{max} is the maximum velocity of particle at a constant time step Δt . For the next N_{verlet} time step, collision detection is based on this list before building a new list [30]. Usually, a combination of grid decomposition and Verlet lists is used. The grid spacing and the skin parameter are optimized to get a fast algorithm [34].

2.6 Software

For simulation we use LIGGGHTS (**LAMMPS Improved for General Granular and Granular Heat Transfer Simulations**) which is an open source software for particle simulation with discrete element method. Discrete Element Methods (DEM) which also as molecular dynamics (MD) is the approach towards the microscopic understanding of macroscopic particulate material behavior using the modeling of particles [36].

LIGGGHTS has several advantages for our aims. The important ones for us here are:

1. Insert an arbitrary geometry

It lets us to import any arbitrary geometry in our simulation. This geometry should be imported as an *STL ASCII* format. This format stores geometry based on triangulation meshes. The related command is **fix mesh/surface**.

2. Vibrate the geometry

We need to have a steady-state vibration in our simulation. The command **fix mesh/surface wiggle** can oscillate our container which imported as mesh through previous command. This vibration can be sinusoidal with arbitrary amplitude in three axis of Cartesian coordinate with our desirable period.

The normal force in LIGGGHTS is considered as:

$$\begin{aligned} F_n &= k_n \xi + \gamma_n \dot{\xi} \\ F_t &= k_t \xi + \gamma_t v_{rel}^t \end{aligned}$$

where k_n and γ_n are:

$$\begin{aligned} k_n &= K_{n,specified} \sqrt{\xi R} \\ \gamma_n &= m_{eff} \gamma_{n,specified} \sqrt{\xi R} \end{aligned}$$

We need to compare above-mentioned equations with Eq.2.8 to find $K_{n,specified}$, $\gamma_{n,specified}$ which leads to:

$$K_{n,specified} = \frac{4}{3} E_{eff}$$

$$\gamma_{n,specified} = \frac{3}{2} \frac{E_{eff} (A_i + A_j)}{2m_{eff}}$$

In order to consider effect of delayed recovery of particles, we use *limitForce on* in the related command in **pair_style gran model**.

For tangential part, the k_t the same as before and we take $\gamma_t = \gamma_n$ as discussed earlier.

Chapter 3

Simulation and Results

Providing a weightless condition such as parabolic flights or sounding rockets for experiments is expensive. Hence, the data is limited. Therefore, we perform a simulation. In this chapter, at first, we verify our simulation with experimental data. Then, we extend our data set with investigation on the effects of vibration, material properties and filling rate on the efficiency of our damper.

3.1 Effect of vibration properties

As mentioned in chapter 1, we focus on the steady-state vibration. In this type of vibration, we continuously apply a sinusoidal displacement to the damper which is :

$$x(t) = A \sin(\omega t)$$

That means the amplitude and frequency of vibration do not change in each period and there is a permanent energy input to the system. There are only two parameters in this kind of vibration: Amplitude and angular velocity. Therefore, we would like to see the effects of these parameters on our damper's efficiency.

3.1.1 Amplitude

Steps taken to simulate are:

- create the a box and import it in LIGGGHTS (see section 2.6).

- define the force explained in the previous chapter and apply vibration. See Appendix A for a sample LIGGGHTS script and the explanation for the commands are in Appendix B. The parameters are in table 3.1.

Parameter	value
Box volume	$50 * 50 * 50 \text{ mm}^3$
Frequency	5 Hz
Young's Modulus(Steel)	203 Gpa
Poisson Ratio(Steel)	0.3
Density(Steel)	$7800 \frac{\text{kg}}{\text{m}^3}$
Coefficient of restitution	0.9
Radius of particle	2 mm
Number of particle	507

TABLE 3.1: Parameters of simulation

We insert particles randomly in the box with zero velocity and then vibrate it for some periods of oscillation (here it is 20 period).

In the figure 3.1 we show the efficiency of the damper for the first 20 periods of oscillation for some amplitudes of vibration. The amplitudes 20,40 and 50 [mm] are in the collect-and-collide regime and the amplitudes 7 and 12 [mm] are in the gaseous regime. After the first period we have almost steady-state for amplitudes in the collect-and-collide regimes since they move as a cluster. But, in the gaseous regime we see some fluctuations mainly because of the random movement of particles in this regime.

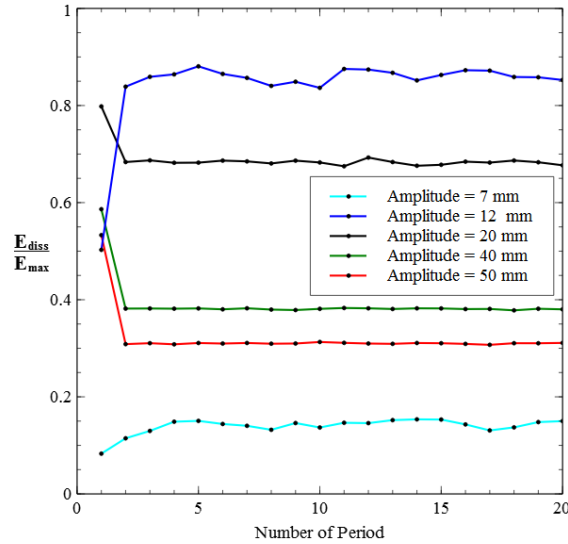


FIGURE 3.1: Simulation results for different regimes after some period to see whether steady-state is remained.

Equation 1.1 calculates the dissipation in one period of oscillation. Figure 3.1 shows some fluctuations in the results. Therefore, to reduce the error, we calculate the dissipation in equation 1.1 for the five last consecutive periods of oscillation in our simulations to decrease the error. Then take an average from them.

Figure 1.6 shows the efficiency of the damper as a function of amplitude of vibration. Therefore, we validate our simulation result with the set of data from experiment [14]. Our results are shown in the figure 3.2. The qualitative behavior is in agreement with figure 1.6 from experiment. However, There are some differences with the experiment quantitative-wise. Therefore, we change one effective parameter, the coefficient of friction which is not measured in the experiment. The result for different coefficients of friction are shown in the figure 3.2. It seems that the value of 0.1 for coefficient of friction has the best fit to our experiment. In this figure, the optimum amplitude in which maximum dissipation happens is 12.8 [mm].

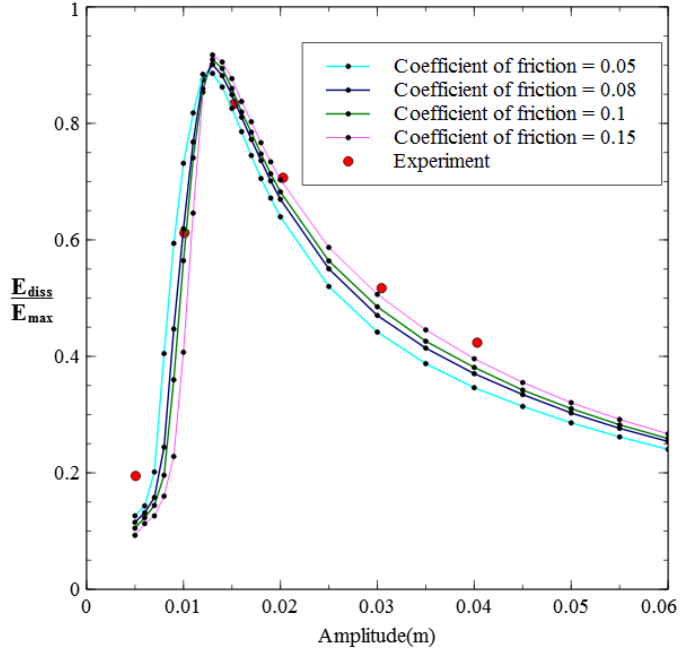


FIGURE 3.2: Efficiency as a function of amplitude

3.1.2 Frequency

Figure 3.3 shows that the efficiency of the granular damper is independent from frequency. Parameters are taken from table 3.1, the amplitude is chosen to be the optimal amplitude in equation 1.6.

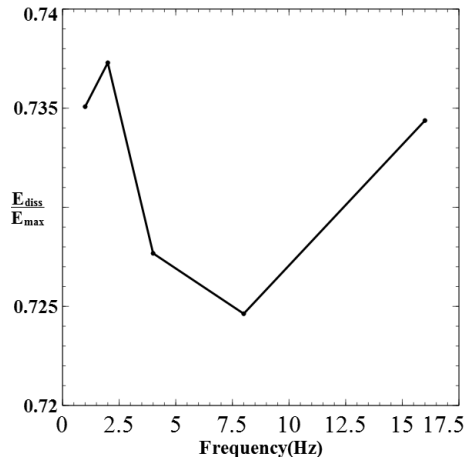


FIGURE 3.3: Efficiency as a function of frequency

We can predict this behavior by considering the single quasi-particle model. With using Eq.1.5 in Eq.1.3, we have:

$$\frac{E_{diss}}{E_{diss}^{max}} = \frac{1}{4} \left[1 - \sin \left(\frac{L_g}{2A} \right) \right]^2$$

Therefore, this model predicts that the efficiency is independent from frequency. Also in the article [14] the authors use different frequencies in their experiment for the granular damper in weightless condition to show that the efficiency of the damper is independent from frequency. However, this result can also verify our simulation.

3.2 Influence of material properties

Our contact force (Eq.2.8 and Eq.2.13) depends on some parameters such as Poisson ratio, Young's modulus, coefficient of restitution, coefficient of friction and particle size. Therefore, it is interesting to observe their influence. We expect that the efficiency of the granular damper is independent from some of those parameters. Nevertheless, we would like to check them.

3.2.1 Poisson ratio and Young's modulus

The impacts of Poisson ratio and Young's modulus are shown in the figure 3.4 for optimum amplitude of vibration in equation 1.6 and the particle and container properties are as mentioned in table 3.1. Figure 3.4 shows that the efficiency of the granular damper is independent from Poisson ratio and Young's modulus. This is because we have an inelastic collapse. The inelastic collapse firstly introduced by *McNamara and Young* [37] in a one-dimensional granular medium. They showed that inelasticity can lead to an infinite number of collisions occurring in a finite time. Therefore, we expect that regardless of their material properties, the energy dissipates through inelastic collapse phenomenon if there are enough layers of grains.

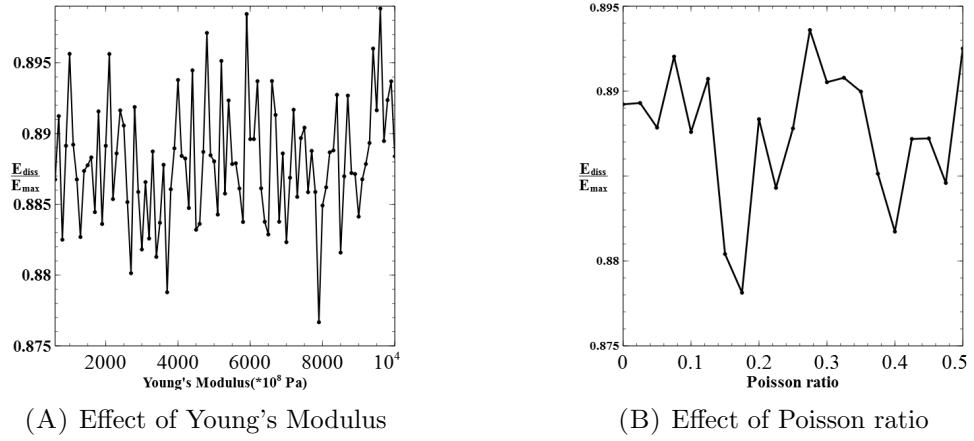


FIGURE 3.4: Effect of Poisson ratio and Young's Modulus on the efficiency of the granular damper at optimum amplitude

Marhadi et.al. [38] experimentally investigated the effect of different particle materials in a particle damper which are attached to a cantilevered beam. Figure 3.5 shows their experimental setup. They have a transient vibration in their experiment.

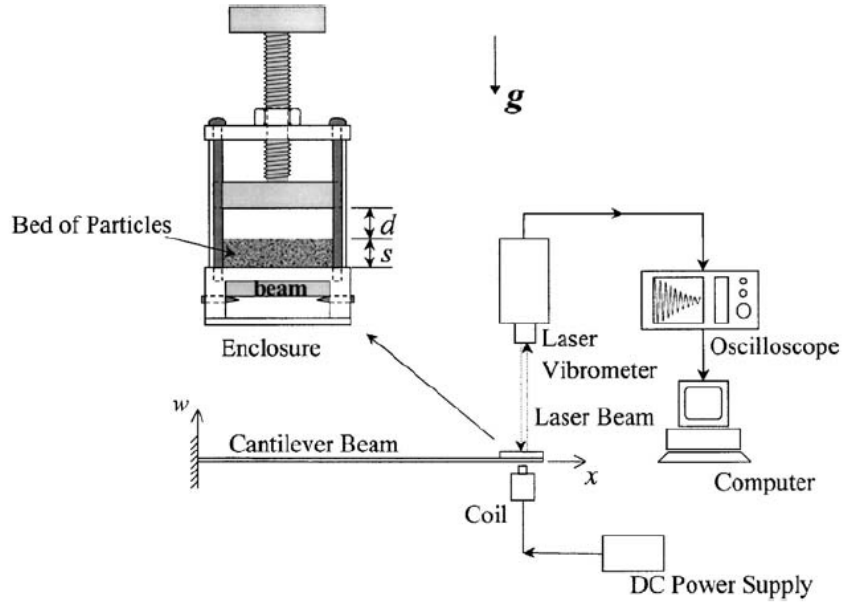


FIGURE 3.5: A schematic of experimental setup in [38] for a particle damper attached to a cantilevered beam.

Specific damping capacity (Ψ) is defined as the kinetic energy converted into heat during one cycle with respect to the maximized kinetic energy of the structure during the cycle,

$$\Psi = \frac{\Delta T}{T} \quad (3.1)$$

where T is given by:

$$T = \frac{1}{2}MV^2$$

where M is the primary mass of the equivalent single-degree-of-freedom system, $M = 0.24\rho AL + m_{encl}$, where ρ is the mass density, A is area of cross-section, and L is the length of the beam and m_{encl} is mass of enclosure [38]. The energy dissipated during an impact can be written as:

$$\Delta T = \frac{1}{2} (1 - \epsilon^2) \frac{m}{1 + \Lambda} (v_p^- - v_2^-)^2 \quad (3.2)$$

where $\Lambda = m/M$ is the ratio of the mass of the particles to the primary mass and v_p^- , v_2^- define as the velocity of particle and the primary mass before an impact. Using Eq. 3.2 in Eq. 3.1 the dimensionless parameters of Eq. 3.1 becomes:

$$\Psi = f(\Lambda, \Upsilon, \Gamma) \quad (3.3)$$

where $\Upsilon = L_g\omega^2/g$ is dimensionless clearance and $\Gamma = A\omega^2/g$ is dimensionless amplitude.

Their results in the figure 3.6 show the mass normalized damping, $\Psi_m = \Psi(1 + \Lambda)^2/\Lambda$ as a function of dimensionless acceleration amplitude, Γ . By comparison the figures 3.6(A), 3.6(B) and 3.6(C) we can clearly see that the effect of material disappears as the number of particles increases (about five layer of particle). In our simulation we have about four layers of particles which can verify with this experiment result.

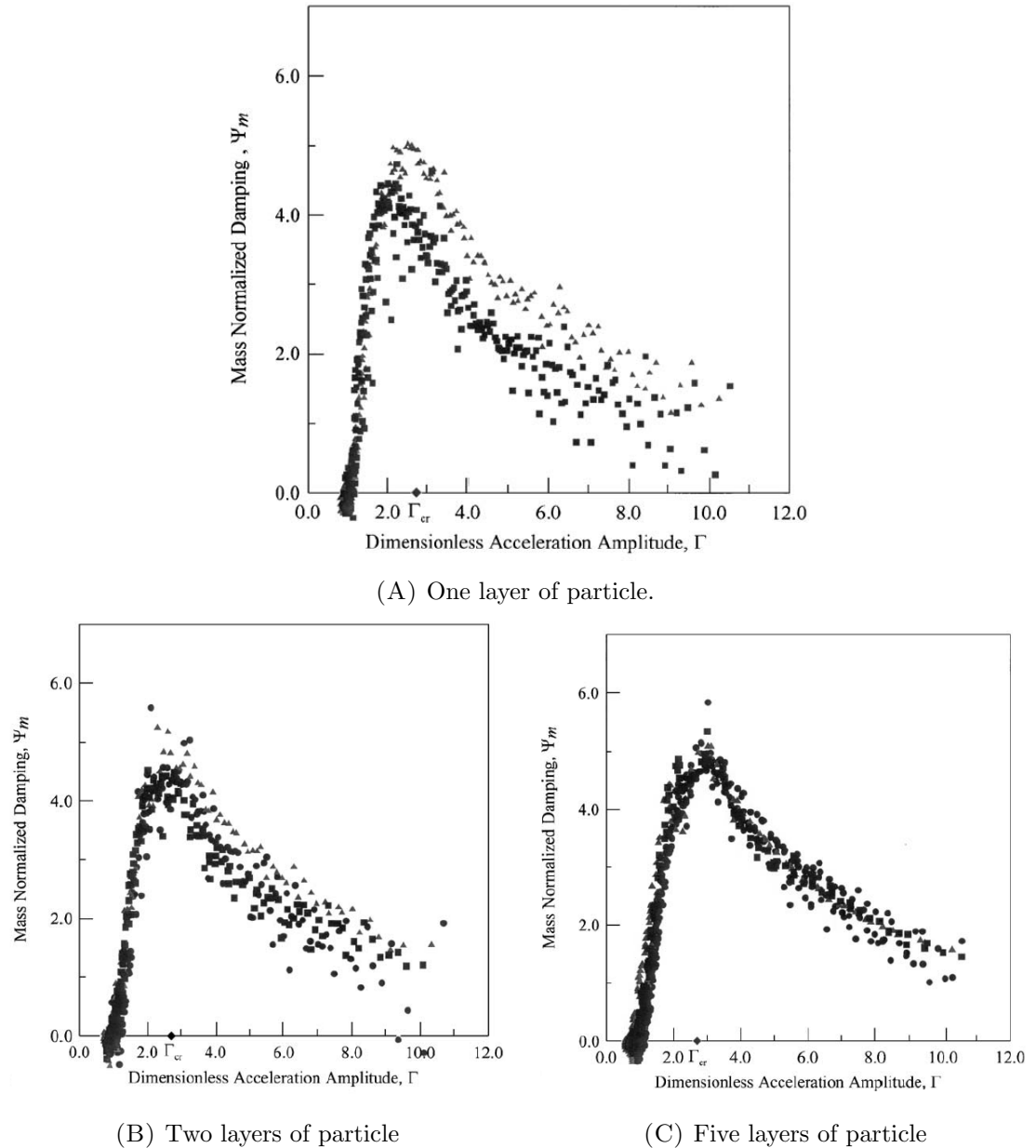


FIGURE 3.6: Comparison of mass normalized damping for three different materials for the same size, shape and number of particles [38]. ▲ lead spheres, ● glass spheres, ■ steel spheres

3.2.2 Coefficient of friction

One effective procedure to dissipate energy is friction between particles. Figure 3.7 shows the efficiency as the coefficient of friction and the amplitude of vibration. The other parameters are kept the same as in table 3.1.

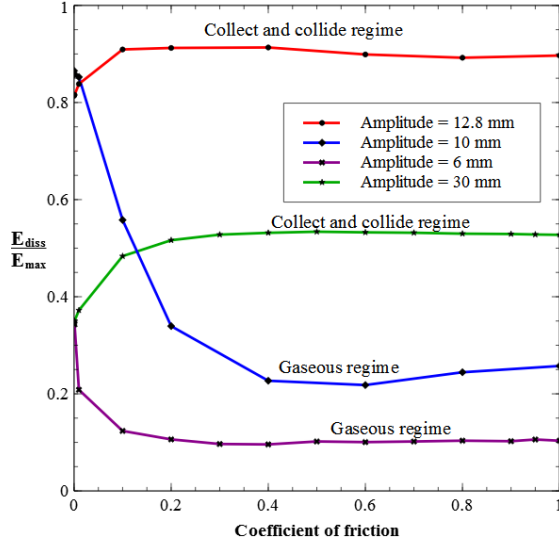


FIGURE 3.7: Effect of coefficient of friction on the efficiency of the granular damper for the collect-and-collide and the gaseous regimes.

The amplitudes 12.8 and 30 [mm] are in the collect-and-collide regime and the amplitudes 6 and 10 [mm] are in the gaseous regime. Results show that in the collect-and-collide regime, first the efficiency becomes better by increasing the coefficient of friction until a threshold and after this threshold the efficiency becomes independent from the coefficient of friction. On the contrary, in the gaseous regime, the efficiency is reduced by increasing the coefficient of friction until a threshold and after this threshold it becomes independent from coefficient of friction similar to collect-and-collide regime.

To understand the reason of this behavior, we look at how the granular damper works. The granular damper mechanism works by first transferring energy to the particles and then dissipate them by particles' interaction through collision and friction. These two steps are independent from each other. *Bai et.al*[5] define the energy dissipation capacity as a maximum energy that can be dissipated in one cycle. With increasing the coefficient of friction the energy dissipation capacity rises but we can not necessarily use all of this capacity and sometimes energy transferring can be a limiting step [5].

Let us first have a look at the result for the collect-and-collide regime. A comparison between the friction part and the frictionless part, shows that the most amount of energy dissipates through collision. Increasing the coefficient of friction, we increase the dissipation capacity but as shown in figure 3.7 there is a threshold for coefficient of friction after which the efficiency becomes almost insensitive to it. The reason is that the the energy transferring is not changed as also mentioned in [5] and it becomes our limiting step and therefore we are in the static regime for friction as explained in previous chapter.

Now let's consider the gaseous regime. Interestingly, with increasing the coefficient of

friction, the efficiency decreases. Visualization of snapshots from simulation are shown in figures 3.8 and 3.9 in a gaseous regime for frictionless and the coefficient of friction 0.6, respectively. The comparison between these figures reveals that particles' speed of collision become reduces and the center of the mass of particles tends to be closer to the center of cavity. However, after threshold it becomes independent from friction like the collect-and-collide regime.

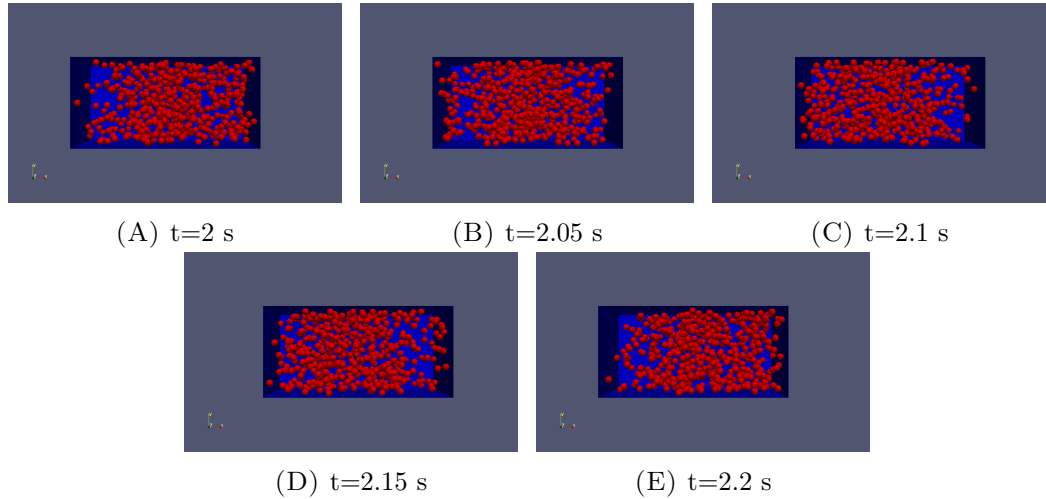


FIGURE 3.8: Snapshots from simulation for the granular damper. The driven amplitude is $6[\text{mm}]$ and the coefficient of friction is zero. The grey area is used to illustrate the position of the damping box within the simulation domain.

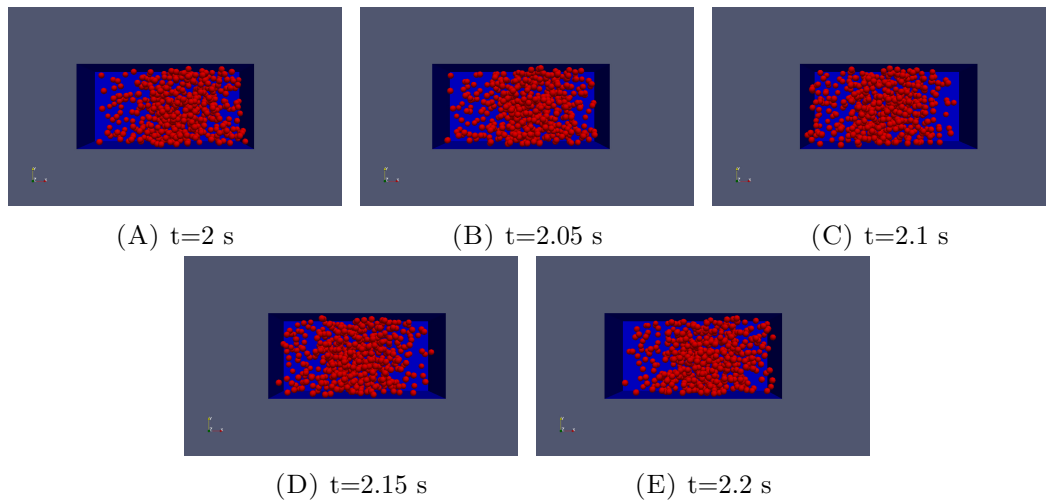


FIGURE 3.9: Snapshots from simulation for the granular damper. The driven amplitude is $6[\text{mm}]$ and the coefficient of friction is 0.6. The grey area is used to illustrate the position of the damping box within the simulation domain.

3.2.3 Coefficient of restitution

The other effective parameter to dissipate energy is inelasticity of collision which appears in the coefficient of restitution. Therefore, we aim to see its effect on the efficiency of our damper.

As in part 3.2.2, we investigate changing the coefficient of restitution in different amplitudes which leads to different regimes. The other parameters are the same as in table 3.1. The optimum amplitude here is 12.8 [mm].

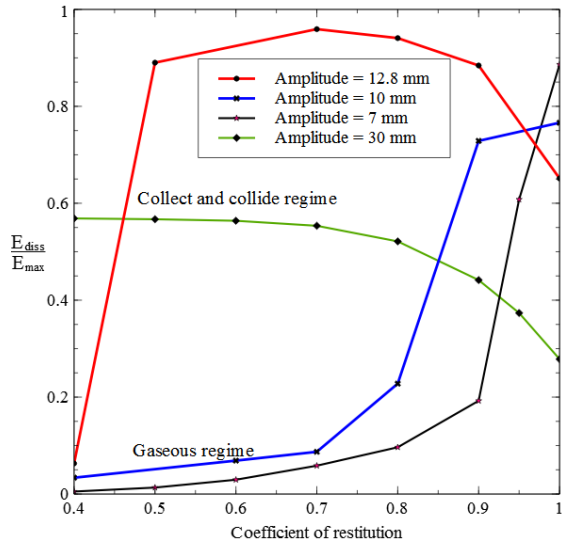


FIGURE 3.10: Effect of coefficient of restitution on the efficiency of the granular damper for different regimes.

The results are shown in figure 3.10. In small coefficient of restitution and small amplitudes of vibration, our result shows very low efficiency while we expect more energy dissipation. From visualization (figure 3.11) we see that our system is almost not working and we can not see collect-and-collide and gaseous regimes. Particles tend to stick together and locate in the middle of container. Therefore, for a relatively long time there is no interaction between container and particles. Hence, we insert energy all the time but the particle can not transfer the energy. However, with increasing the coefficient of restitution our mechanism starts to work effectively.

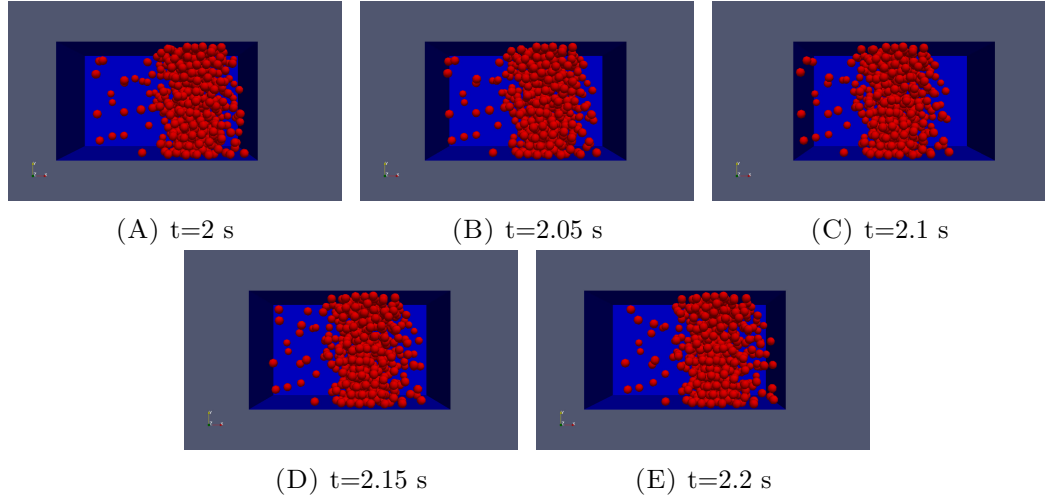


FIGURE 3.11: Snapshots from simulation for the granular damper. The driven amplitude is 7 [mm] and the coefficient of restitution is 0.4. The grey area is used to illustrate the position of the damping box within the simulation domain.

Increasing the coefficient of restitution means that less energy dissipates by a single collision of particle-particle or particle-wall interaction. But, the probability of having higher number of collisions in a specific time, increased.

For the amplitude of 12.8[mm], after the coefficient of restitution gets about 0.5 the system works properly. Having the coefficient of restitution in the range of 0.5 and 0.9, the efficiency slightly changes. However, after that the efficiency reduces. Through visualization of simulation we understand that the system has a tendency towards gaseous behavior (compare figure 3.12 and figure 3.13). Therefore, the efficiency has reduced. The coefficient of restitution one is also a point of interest. We expect that the efficiency becomes almost zero since impacts are completely inelastic. The reason for having high value of dissipation here is that we have a friction. In a frictionless condition it becomes almost zero as we checked.

For amplitude less than 12.8 [mm], with increasing the coefficient of restitution the efficiency becomes better. In this regime, particles' speed are low and the small coefficient of restitution has the same effect like collect-and-collide regime for small one. With increasing the coefficient of restitution, the system mechanism works properly.

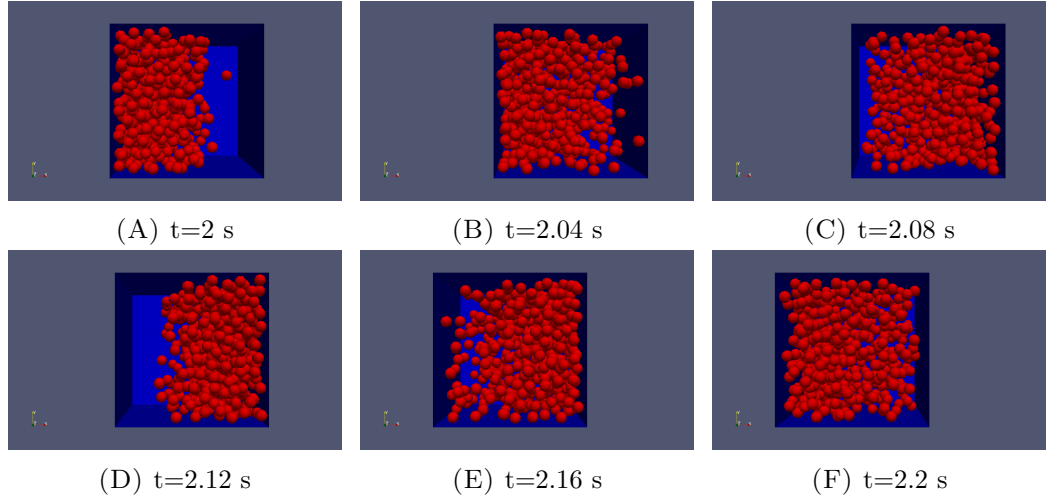


FIGURE 3.12: Snapshots from simulation for the granular damper. The driven amplitude is 12 [mm] and the coefficient of restitution is one. The grey area is used to illustrate the position of the damping box within the simulation domain.

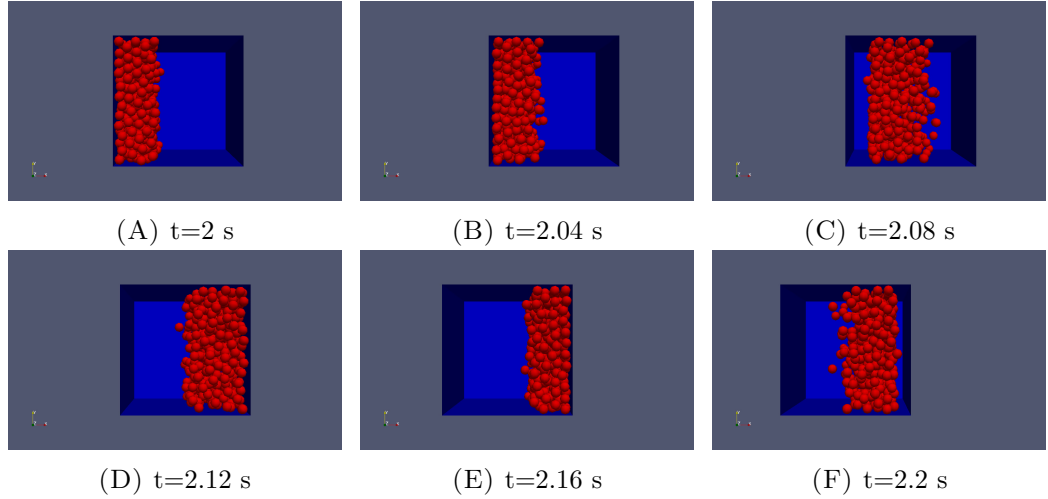


FIGURE 3.13: Snapshots from simulation for the granular damper. The driven amplitude is 12 [mm] and the coefficient of restitution is 0.7. The grey area is used to illustrate the position of the damping box within the simulation domain.

3.3 Filling ratio

The effect of number of particles with conserving the mass can also be interesting. For conservation of the mass, we just need to have a correct correlation between number and size of particles:

$$\frac{N_1}{N_2} = \left(\frac{r_2}{r_1}\right)^3$$

where $N_{1,2}$ and $r_{1,2}$ are the number of particles and the size of them in two different distribution.

Except for the number, radius of particles and the coefficient of friction which is zero here, the other parameters are same as in the table 3.1. The amplitude of vibration is 12.8[mm].

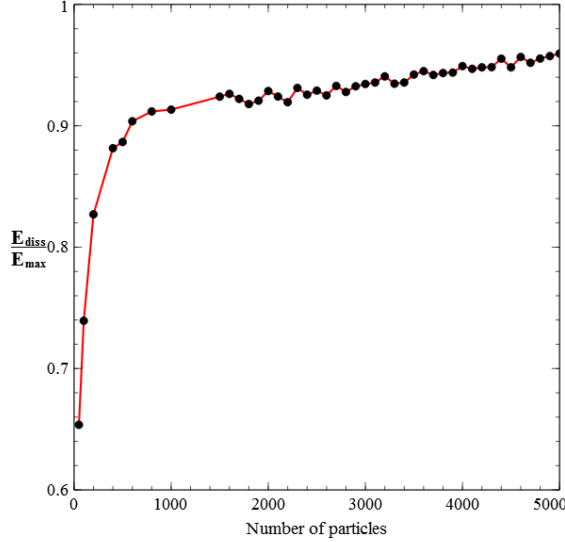


FIGURE 3.14: Effect of granularity on the granular damper at optimum amplitude.
The number of particles and adapt the size of them to conserve the mass in total.

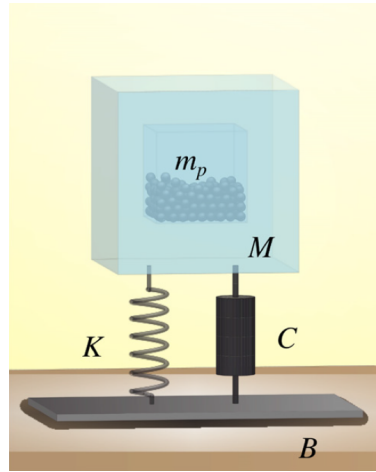
Figure 3.14 shows that with increasing the number of particles the efficiency of damper become better. However, after some number of particles (which here is about 1000 particles), we almost have enough layers of particles (which here is about four layers) that elastic collapse happens properly. After about 1000 particle, the efficiency of damper slightly increased.

There are two possible explanations for increasing the efficiency with increasing the number of particles. One is that there are less spaces between smaller particles [39]. This can affect the packing of particles which is related to the L_g as one of the important parameters that play a role in the efficiency of the granular damper as discussed in the first chapter. Generally, the rigidity and flow characteristics of a granular material are determined by the geometrical packing of its particles [17]. In general, it can be shown that monodisperse spheres can be arranged in space from simple cubic to close-pack in a symmetric way. Ideally, pack density for these two types are 53.36% and 74.05%, respectively [39]. But in our work, the grains will form a disordered structure. The loosest way to pack spheres (random loose packing, RLC) gives a density of $\approx 55\%$. The maximum random packing density (random close packing, RCL) is $\approx 64\%$ [40]. It is worth to mention that recent study shows that the random packing of monodisperse hard spheres in three dimensional can pack between the densities $\approx 53.6\%$ and $\approx 63.4\%$.

[41].

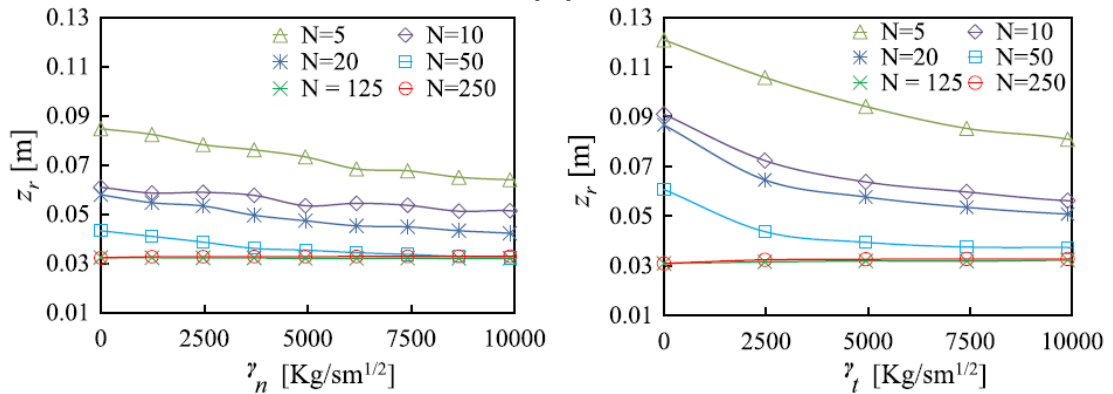
The other reason is that decreasing the size of particles, the number of particles and therefore collisions increased and may lead to a complete perfect inelastic collapse that dissipate the entire energy.

The effective inelastic collapse phenomenon can be seen in the study of *Sánchez et al.* [42]. They investigated on the effect of granular interactions on the response of a granular damper by means of numerical simulation in the steady state vibration. They observed a universal response over a wide range of working conditions and explained this behavior in terms of inelastic collapse.



(A) Schematic of a particle damper in

[42]



(B) The vibration amplitude Z_r at resonance as a function of the collisional dissipation γ_n and γ_t for different number N of grains in the enclosure [42].

FIGURE 3.15: Simulation setup and response of amplitude of vibration for different number of grains in [42].

Their result in figure 3.15(B) shows the frequency function response which means the amplitude of vibration z_r at the resonant frequency as a function of normal (γ_n) and tangential (γ_t) dissipative parameters for different number of particles. We can see that whenever the number of particles exceeds from 100 particles, a constant (universal)

response is recovered [42]. They estimated from their simulations that whenever the layers of particle exceed from three or more layers in the container, the system response near resonance becomes independent of the particle–particle interaction. Based on this explanation, we expect that after a specific layer, our response becomes independent from number of particle while clearly we have a slight slope in the figure 3.14 and it can be a potential question for the future work.

Chapter 4

Optimization

In this chapter we would like to find the methods for improving the granular damper that works on a wide range of amplitudes efficiently. For instance, figure 4.1 shows the efficiency of the granular damper. We would like to improve this efficiency so that it covers a wide range of amplitudes efficiently which is shown there as goal.

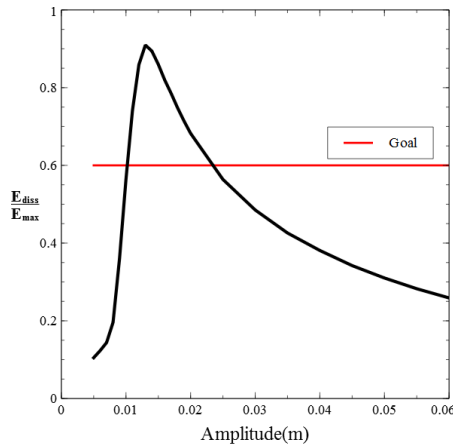


FIGURE 4.1: Schematic of improving granular damper to work efficiently on a wide range of amplitudes.

Therefore, we try two methods. The first one is using a multicomponent damper and the second one is changing the shape of cavity.

4.1 Multicomponent damper

Jadhav et.al.[43] by means of experiment showed that the multiple cell enclosure can enhance the performance of particle damping. They tested both single cell (see figure

4.2(A)) and multiple cell (see figure 4.2(B)) enclosure with keeping the mass of particles constant.

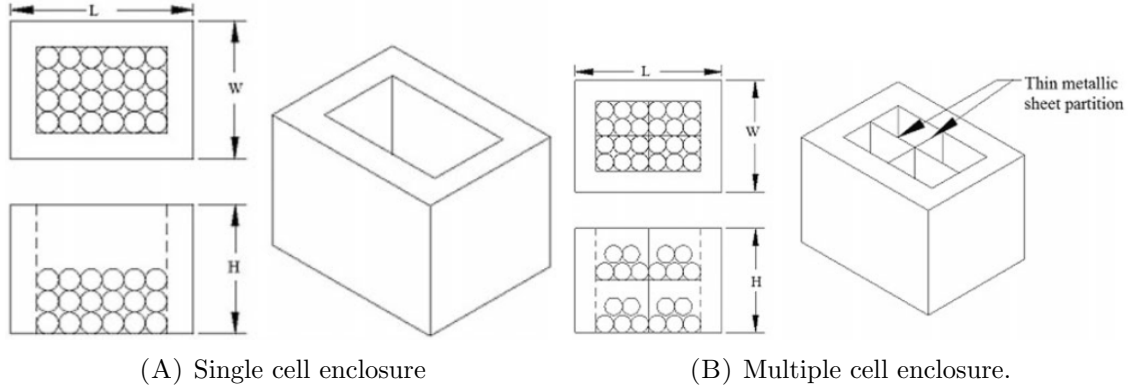


FIGURE 4.2: Single and multiple cell enclosure. Pictures are taken from article [43]

They attached these particle-filled enclosures to the free end of a cantilever beam with the exciter to produce a steady state vibration(see figure 4.3(A)). The result in figure 4.3(B) illustrates the frequency response for the beam without particle damper, single cell particle damper and multiple cell enclosures. It can be seen that the single cell particle damper reduced the amplitude of vibration about 55 to 60 % compared to the beam without damper and additionally 18 to 24 % reduction in vibration amplitude is gained by using a multiple cell enclosure. Thus, it is possible to maximize the damping effectiveness using less damping material with the multiple cell enclosure [43].

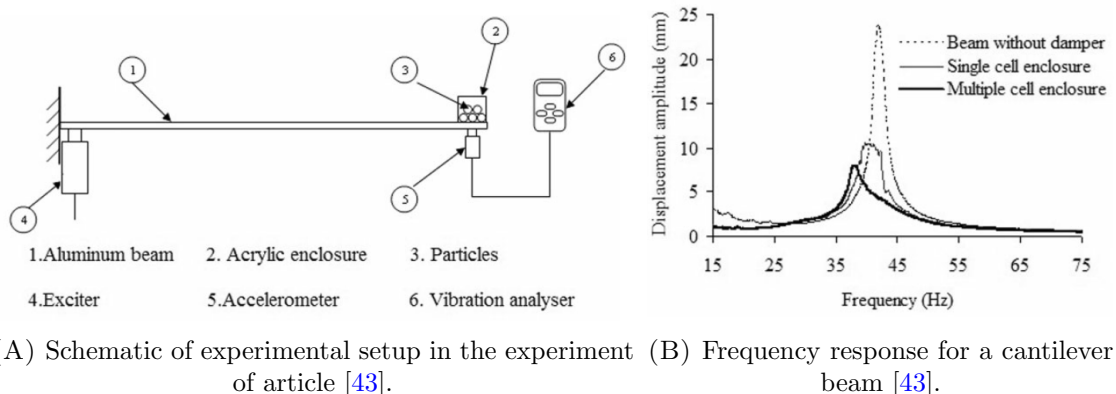


FIGURE 4.3: Experimental setup and result of frequency response of a granular damper in a cantilever beam [43].

The previous study has used only eight cells. There are other investigations on the effect of the number of cavities. One of the studies has been done by *Saeki* [44]. He investigated the performance of a multi-unit particle damper in a horizontally vibrating system by means of experiment and analytic (see figure 4.4(A)).

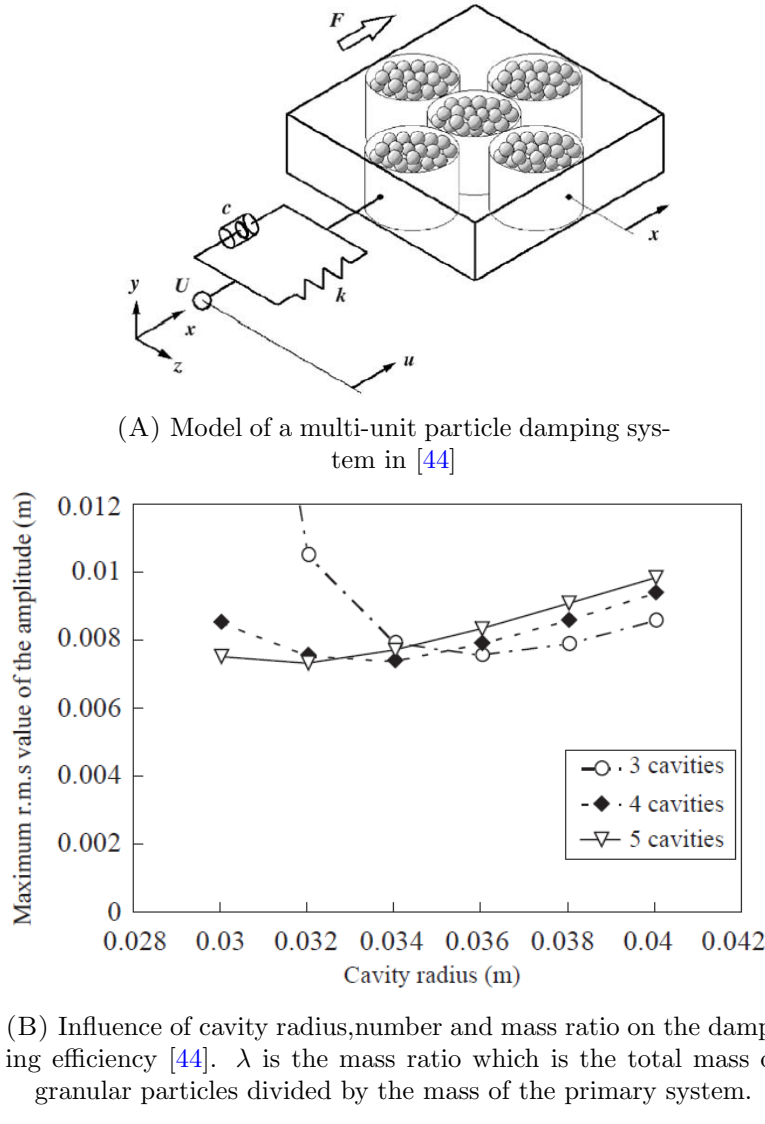


FIGURE 4.4: Experimental setup and effect of cavity properties on the maximum root mean square(rms) value of the amplitude of the oscillation [44].

Figure 4.4(B) shows the effect of the unit number on the optimum cavity radius. The effect of the cavity radius on the maximum rms value of the primary system amplitude is more significant as the unit number decreases [44]. The maximum rms values of the primary system amplitude at the optimum cavity radius are almost the same. In addition, the optimum cavity radius decreases with increasing unit number [44]. The reason is that the mobility of granular particles in a cavity increases as the unit number increases [44].

Therefore, we use the idea of a multicomponent granular damper to find an optimum damper that can work on a wide range of the amplitudes of the oscillation efficiently. Consider a granular damper like figure 4.5(A) as a base damper. Now assume that we want to have a damper similar to figure 4.5(B) as a multicomponent damper.

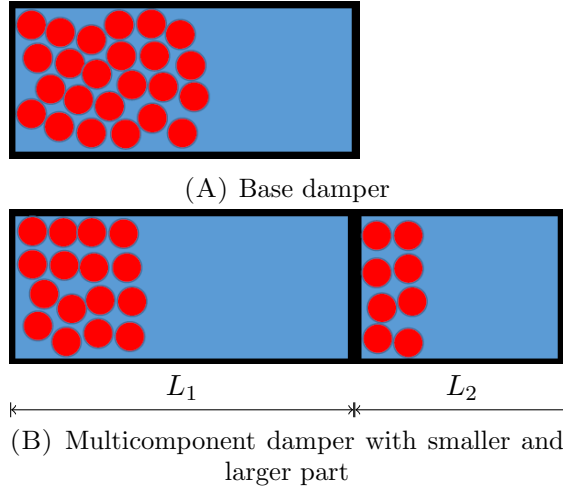


FIGURE 4.5: Front view of base damper and multicomponent damper. The length of base damper is also equal to L_1

We divide particles of base damper in the two containers of figure 4.5(B) based on their length ratio which we define as the length of second component to the length of base unit, L_2/L_1 . Therefore, the total mass is the same in both cases.

$$M_{total} = M_1 + M_2$$

$$\frac{M_2}{M_1} = \frac{L_2}{L_1}$$

There was a bug in LIGGGHTS when the thickness of wall between components was zero. For more explanation see appendix C. Now if we assume that the multicomponent damper consists of separate containers which vibrate with the same condition simultaneously, we expect that the total dissipation energy becomes :

$$E_{diss} = \sum_{i=1}^n \int_T \dot{x}(t) f_i(t) dt$$

Where n is the total number of dampers. The maximum energy dissipation defines as:

$$E_{max} = 4M_{total} A \omega^2$$

where $M_{total} = \sum_{i=1}^n m_i$ is the total mass of particles.

We expect that knowing the behavior of each damper separately we can find the behavior of combination of them.

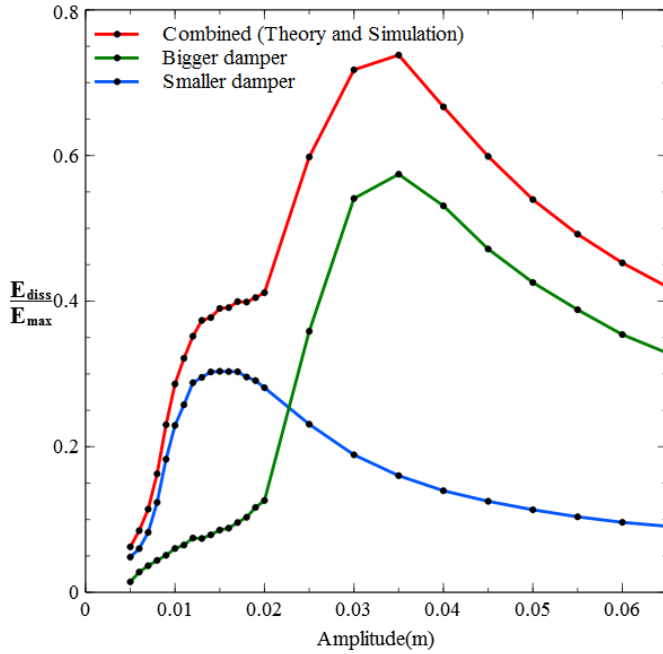


FIGURE 4.6: The combined dampers can have same result when we add them separately

For instance, we create a multicomponent damper with two units and compare it with the result of two separate units. For simulation we use 600 particles with the coefficient of friction 0.05 and $L_1 = 60[\text{mm}]$ the other parameters are same as in table 3.1. Figure 4.6 shows that we can use the superposition to find the multicomponent efficiency. The peak performance of multicomponent damper tends toward the component which has more mass. Therefore, here it closes to the bigger damper which has larger L_g and therefore larger optimum amplitude $A^{opt} = L_g/\pi$.

Now we would like to see the effect of different length ratios which defines as length of new component to length of base component. Figure 4.7 shows the efficiency of multicomponent damper for different length ratios. For the ratio smaller than one, the model is not useful because the peak performance is low and also the graph become narrower. However for the ratio larger than one it becomes more effective and the graph becomes wider to cover more amplitudes.

The amplitude of the peak performance of each multicomponent damper in figure 4.7, increased when the length ratio increased. As discussed earlier, the peak of each graph tends toward the component which has more mass inside it. Therefore, as the ratio increased, the bigger component has more particles but it has large L_g in our cases. Hence, the optimum amplitude $A^{opt} = L_g/\pi$ increased for components which have large length ratios.

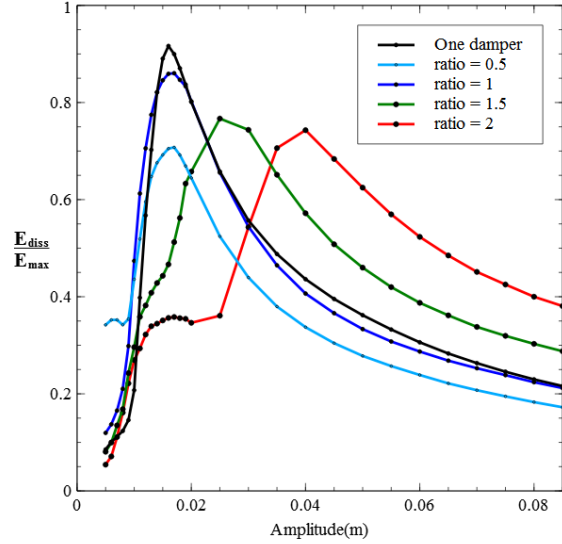


FIGURE 4.7: Combination of two dampers with different length ratios

Now we increase the number of dampers with three parts like in the figure 4.8.

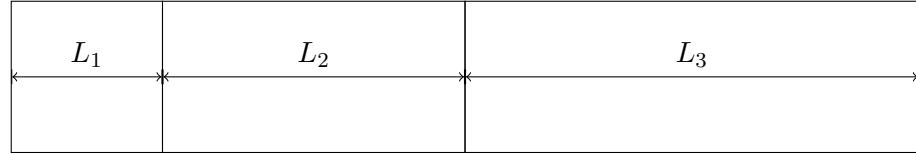


FIGURE 4.8: A three part damper. The length ratios of dampers are: $\frac{L_3}{L_1} = 3, \frac{L_2}{L_1} = 2$

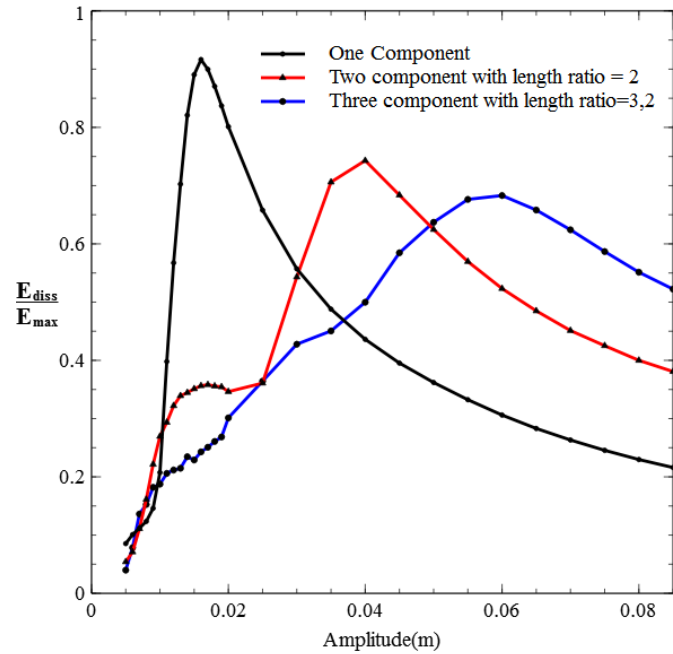


FIGURE 4.9: Comparison of one, two and three component dampers

Figure 4.9 shows that increasing the number of units with defining the mass inside them based on their length ratio may reach to our goal for covering a wide range of amplitudes efficiently. For instance, the range of amplitudes that have an efficiency of 60% and more are: $12\text{mm} < A_1 < 27\text{mm}$, $32\text{mm} < A_2 < 52\text{mm}$ and $46\text{mm} < A_3 < 73\text{mm}$ for one, two and three part damper, respectively. Clearly, the three component damper covers a wider range of amplitudes.

In the other simulation we try to use a multicomponent damper with 28 units. The length of each unit is in the range of 28[mm] to 198[mm] ($L_1 = 28, L_2 = 35, \dots, L_{27} = 192, L_{28} = 198$). There are 600 particles in each unit and the other parameters are in table 3.1.

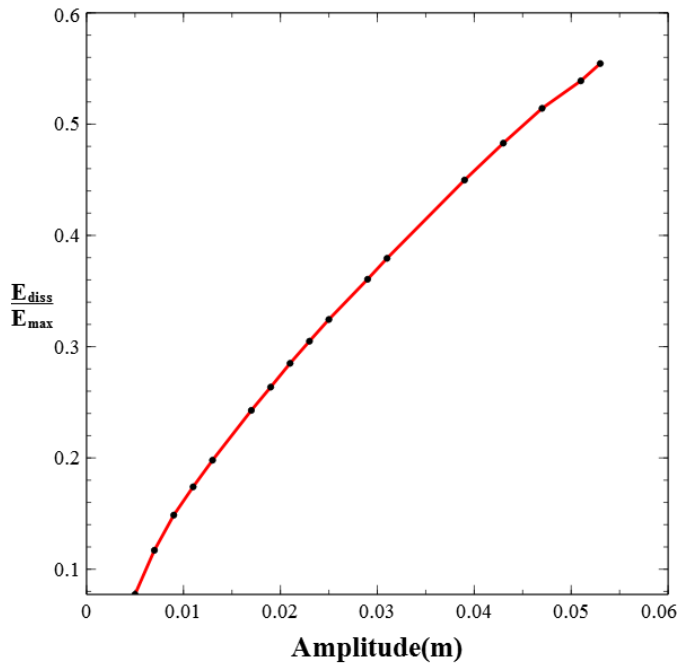


FIGURE 4.10: Efficiency as function of amplitude for a multicomponent damper with 28 units.

The result in figure 4.10 shows that the efficiency continuously increases as the amplitude goes up. It is on the ground that increasing the amplitude results in an increase in the number of components in the collect-and-collide regimes and therefore the efficiency becomes better.

4.2 Complex cavity geometry

It is of interest to know the influence of boundary which here is container's geometry. The effect of enclosure geometry on particle damping performance has been studied by

Wong et.al. [45]. They investigated by means of numerical simulation on the effect of enclosure shape by interpolation between a number of prototype shapes (see figure 4.11).

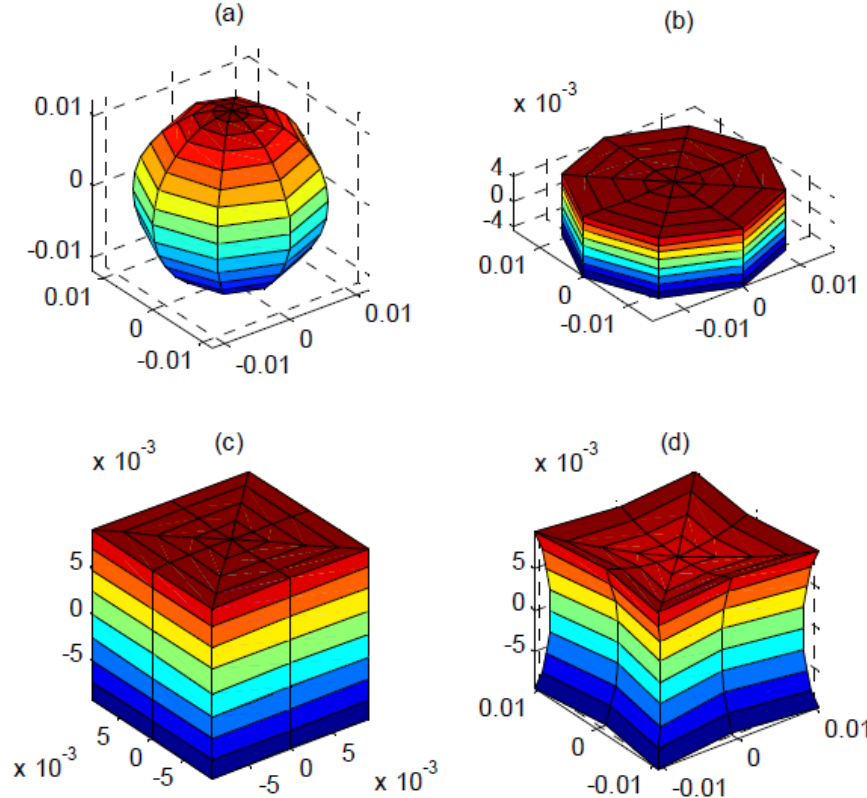


FIGURE 4.11: (a) sphere (b) disc (c) cube are the prototype shapes.(d) interpolated shapes [45].

They have shown that tuning the shapes does play a strong effect in affecting the qualitative performance of the particle dampers. However, their work can not show how to create better and new particle dampers and this is a complex issue.

The effect of geometry also can be seen in the work of *Pacheco-Vázquez et. al.* [46]. They investigated the rebound of cylindrical and spherical containers which are partially filled with the granular materials. The kinetic energy of the container is partially transferred to the grains during the collision, the rebound is damped and the fast energy dissipation through inter-particle collisions and friction decrease the bouncing time considerably. For cylindrical container, a completely inelastic collision (zero rebound) is obtained when $m_i \geq 1.5\epsilon_0 m_c$ where ϵ_0 , m_c and m_i are the coefficient of restitution, mass of the container and mass of grains, respectively. While for the spherical container the first rebound is almost undamped, but the second collision is totally inelastic if $m_i \gg m_c$.

The previous discussions show that the geometry of container can change the granular

damper performance. However, there are some difficulties to analyse different containers. For instance, one difficulty here is that we have not enough constrains to compare our results to other shapes fairly. As an example, the L_g can be different for cube and sphere and we observed that it affects the efficiency. However, we create different geometries somehow that all have the same volume. Our base shape for comparison is cube which is mentioned in table 3.1.

First we start with hour-glass type shapes as can be seen in figure 4.12. We create two shapes with different ratio of $\frac{d_1}{d_3}$ which is one and two for each case of simulations. The ratio of $\frac{d_2}{d_3}$ equals to two in both case of simulations.

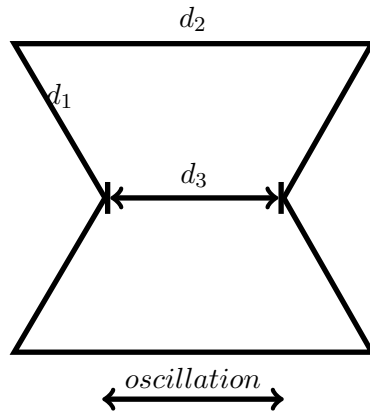


FIGURE 4.12: Front view of hour-glass

Figure 4.13 shows that with increasing the ratio of $\frac{d_1}{d_3}$, the efficiency decreases. The behavior becomes like two separate shapes as the ratio increases. Therefore, we expect that the efficiency of damper becomes worse.

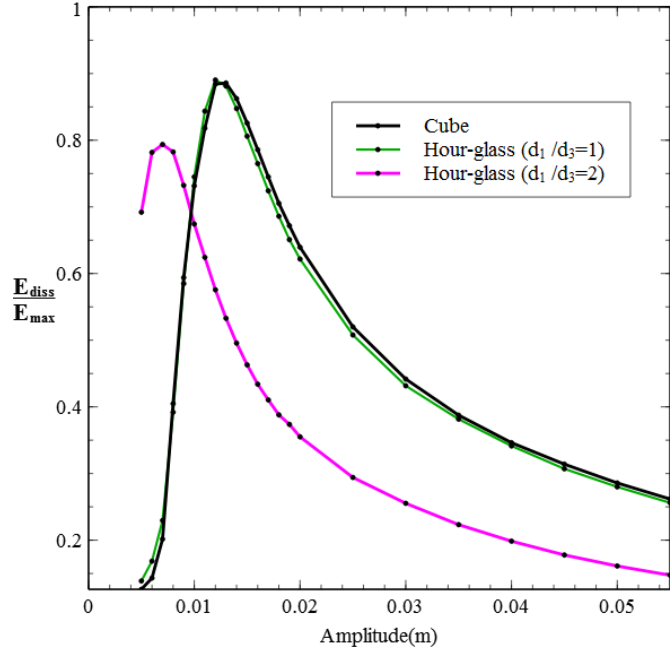
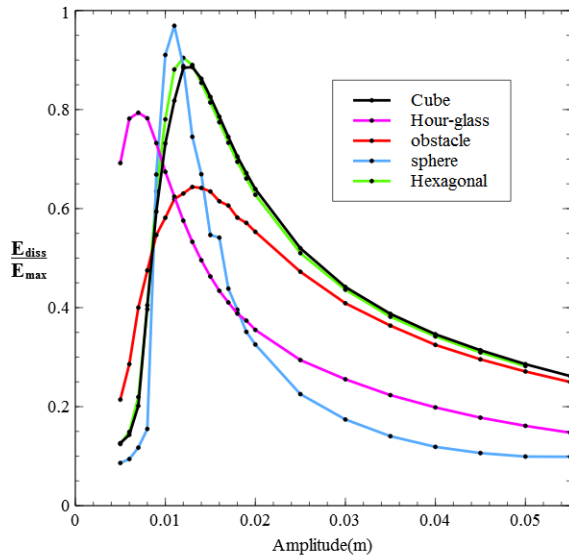
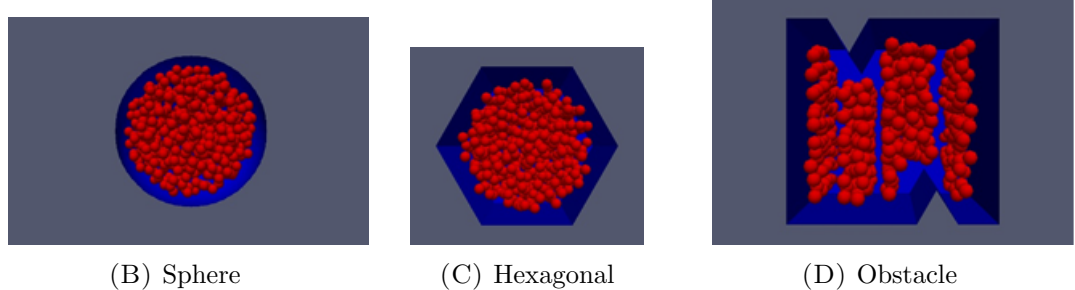


FIGURE 4.13: comparison of the efficiency of damper for the cube container and the hour-glass container with the different ratio of $\frac{d_1}{d_3}$

The previous result shows that the shape mainly changes the performance of the granular damper but may not lead to our goal for working efficiently on a wide range of amplitudes. However, we investigate the effect of sphere, hexagonal and obstacle. All results are shown in figure 4.14(A). Obstacle clearly reduces the efficiency because they corrupt the motion. The interesting shape is sphere. It has the maximum efficiency along all of our shapes. But it is not a robust model and also if our system works on collect-and-collide regime it becomes the worst model among them.



(A) efficiency for different geometry.
All of them have same volume, depth
and mass.



(B) Sphere

(C) Hexagonal

(D) Obstacle

FIGURE 4.14: Effect of different geometries on the efficiency of the granular damper.

Chapter 5

Conclusion

A granular damper is a container which is partly filled with granular materials which may be attached to a vibrating machinery to attenuate the oscillation. In the presence of gravity, the dynamical behavior can be seen as solid, convective and gaslike phases [13]. An efficient operation of granular damper is expected when the average kinetic energy of the particles is larger than their average potential energy which motivated others to perform experiments under weightless condition [6]. Experiments reveal two different dynamical regimes in the weightless condition: gaseous and collect-and-collide regimes. However, providing a weightless condition such as parabolic flights or sounding rockets for experiment is expensive. Therefore, the data set is limited. Thus, we perform simulations to extend our data sets. At first we verify our result with existing experimental data. Then, we investigate the effect of materials and vibration properties. The result shows that the efficiency of the granular damper is independent from frequency, Youngs modulus and Poisson ratio. But it is weakly dependent on coefficient of friction and the coefficient of restitution. It has been shown that if we have five or more layers of particles, the inelastic collapse phenomenon works properly. However, with increasing the number of particles the efficiency continuously becomes better which is unexpected since we expect that it becomes independent from number of particles after a specific number of particles. This behavior remains as a question for future studies.

We try to optimize the granular damper which covers a wide range of amplitudes of vibration. Our first method was using a multicomponent damper. A multicomponent damper consists of two or more units of damper. Our result shows that the efficiency of a multicomponent damper can be found by adding the efficiency of each component independently. Our result also shows that with increasing the number of units with proper mass ratio between them, we can find an appropriate damper which covers a wide range of amplitudes efficiently. The other possible future work is to find a multi-component damper which works almost uniformly in the wide range of amplitudes. This

is a complex and challenging work since the efficiency is nonlinear and damper can work in the different regimes simultaneously.

We also try to see the effect of geometry. The comparison between different shapes can unfairly. For instance, one of the effective parameters, gap length, is changed in different shapes. However, changing the shape was not useful to cover a wide range of amplitude when we use them to conserve the volume. The possible future work is to find the effective gap length for an arbitrary geometry.

Appendix A

LIGGGHTS Sample Script

```
atom_style granular
atom_modify map array
boundary m m m
newton off
communicate single vel yes
units si
processors 1 1 1
region reg block 0.0 0.01 0.0 0.01 0.0 0.01 units box
create_box 1 reg
neighbor 0.005 bin
neigh_modify delay 0
#Material properties required for new pair styles
fix m1 all property/global younghModulus peratomtype 203.e8
fix m2 all property/global poissonsRatio peratomtype 0.3
fix m3 all property/global coefficientRestitution peratomtypepair 1 0.9
fix m4 all property/global coefficientFriction peratomtypepair 1 0.1
fix KN all property/global kn peratomtypepair 1 168498168498
fix KT all property/global kt peratomtypepair 1 208144796380
fix GammaN all property/global gamman peratomtypepair 1 448428791.6
fix GammaT all property/global gammat peratomtypepair 1 448428791.6
#New pair style
pair_style gran model hertz/stiffness tangential history limitForce on
pair_coeff * *
timestep 1e-7
fix cad all mesh/surface file Rectangle.stl type 1 scale 0.001
#region for particle insertion
```

```

region bc block 0.003 0.047 0.003 0.047 0.003 0.047 units box
group nve_group region reg
#distributions for particle insertion
fix pts1 all particletemplate/sphere 100000 atom_type 1 density constant 7800
radius constant 0.002
fix pdd1 all particledistribution/discrete 100000 1 pts1 1.0
#particle insertion
fix ins nve_group insert/pack seed 100000 distributiontemplate pdd1 &
    maxattempt 2000 insert_every once overlapcheck yes all_in yes &
    vel constant 0.0 0.0 0.0 region bc particles_in_region 507 ntry_mc 10000
# apply vibration
fix move all move/mesh mesh cad wiggle amplitude 0.013 0.0 0.0 period 0.2
fix walls all wall/gran model hertz/stiffness tangential history mesh store_force
yes n_meshes 1 meshes cad
# apply nve integration to all particles that are inserted as single particles
fix integr nve_group nve/sphere
thermo_style custom step atoms vol
thermo 200000
thermo_modify lost ignore norm no
compute_modify thermo_temp dynamic yes
#run until steady case
run 20000000
# compute the total force on each time step
compute fore_summation all reduce sum f_force_walls[1]
# store the total force in one variable
variable fs equal c_fore_summation
# compute the wall velocity
variable velocity equal -1*cwiggle(-0.013,0.013,0.2) # compute the dissipation value
for integral
variable dissipation equal v_velocity*v_fs
# store the dissipation ( we multiply it with ω latter.)
fix Dissipation all print 1 "$dissipation" file dissipation.txt screen no
# Use the following command for simulation. But we need to use "pizza.py" to change
in format which readable in "paraview"
dump dmp1 all custom 10000 post/dump*.damper id type x y z
dump dmp2 all mesh/stl 10000 post/dump*.stl cad
run 30000000 upto
write_restart last-simulation.txt
run 1

```

Appendix B

LIGGGHTS commands

B.1 LIGGGHTS ¹

Scripting in LIGGGHTS have four steps:

1. Initialization
2. Atom definition
3. Setting
4. Run a simulation

The last two steps can be repeated several times. There are a lot of commands for each steps. Here we shortly mention on those which have been used in the simulation. For complete description see the documentation of LIGGGHTS.

B.1.1 initialization

In initialization we define parameters which need before create atoms. The following commands are used for this part in the simulations.

- **atom_modify:**

Modify the properties of atom style.

- **atom_style:**

Define which style of atoms uses in the simulation.

¹Explanation are token from LIGGGHTS manual documentation.

- **boundary:**

Set the style of boundaries for the simulation box.

- **newton:**

Turns the newton third law on or off for pairwise and bounded interaction.

- **processors:**

Indicate how processors are mapped as a three dimensional logical grid to the global simulation box.

- **pair_style:**

Set the formulas use to compute pairwise interaction.

- **units :**

Fix the type of units used for a simulation.

B.1.2 Atom definition

The related commands are:

- **region:**

Defines a geometric region of space.

- **create_box :**

Create a simulation box based on the specified region.

B.1.3 Settings

When atoms and molecular (Granular particles in our case) topology are defined, a various of setting can be specified. The relevant commands are :

- **compute_modify:**

Modify one or more parameters of a previously defined compute.

- **compute reduce:**

A calculation that *reduces* one or more vectors inputs into scalar values.

- **dump:**

A snapshot of atom quantities to one or more files at every specific time steps.

- **fix insert/pack:**

Insert granular specified number of particles in a specific region at once or every few time steps.

- **fix mesh/surface:**

Let to import of triangular surface mesh wall geometry for granular simulations from ASCII STL files

- **fix move/mesh:**

Update the position and velocity for mesh elements from *fix mesh/ surface*

- **fix nve/sphere:**

Perform a constant NVE integration to update position,velocity and angular velocity for a spherical particles in the group at each time step.

- **fix print:**

Use this command to write the suitable variable in a file for further analysis.

- **fix property/global:**

Reserves global properties to be access by user or other or fixes or pair styles

- **fix particledistribution/discrete:**

Define a discrete particle distribution and take *fix particletemplate/sphere* as an input which define a properties of a single particle.

- **fix particletemplate/sphere:**

Define a particle that is used in *fix particledistribution/ discrete*.

- **fix wall/gran:**

Bound the simulation domain of a granular system with a frictional wall.The equation for the force between the wall and particles that interact it, is same as the corresponding on the pair_style.

- **group:**

Identify a collection of atoms that belong to a group.

- **neighbor:**

Set parameters that affect the building of pairwise neighbor lists.

- **neigh_modify:**

Set parameters that affect the building and use of pairwise neighbor lists.

- **pair_coeff:**

Specify the pair wise force field coefficients for one or more pairs of atom types.However, for granular style there are no additional coefficient need.

- **thermo:**

Print the thermodynamic information which controlled by *thermo_style* and *thermo_modify* at every specific number of time steps.

- **thermo_modify:**

Set options how thermodynamic information is computed and printed.

- **thermo_style:**

Style and content of thermodynamic data to print on screen and log file.

- **timestep:**

The time step size.

- **variable equal:**

Assigns one or more strings to a variable name for evaluation later in the input script or during a simulation.

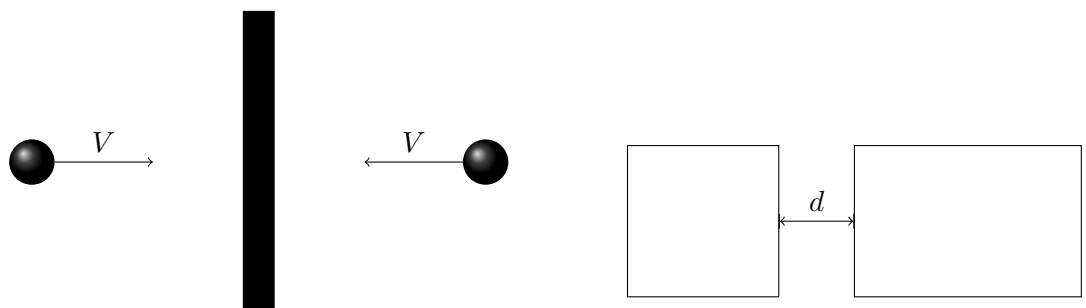
B.1.4 Run a simulation

A molecular dynamics simulation is run with command "run". After this command, we specify the number of time step that we need for simulation.

Appendix C

LIGGGHTS bug

At the time when we run the simulation, there was a bug in the LIGGGHTS. The bug is that if we have a wall with zero thickness and two particle impact with it in a completely symmetric condition like figure C.1(A), the coefficient of restitution will not be the same as we defined in commands. Thus, we create a distance, similar to figure C.1(B), to make sure that this problem does not affect our result.



(A) Two particle impact on a wall with completely symmetric condition
(B) Front view of combination of two damper. There is a distance d in between walls to prevent the bug in simulation.

FIGURE C.1: Schematic of the bug in the LIGGGHTS and a solution to prevent it.

Bibliography

- [1] H.M. Jaeger, S.R. Nagel, and R.P. Behringer. The physics of granular materials. *Reviews of Modern Physics*, 1996.
- [2] H.M. Jaeger and S.R. Nagel. Granular solids, liquids and gases. *Reviews of Modern Physics*, 68(4):1259, 1992.
- [3] R.D. Friend and V.K. Kinra. Particle impact damping. *J.Sou.Vib.*, 233:93, 2000.
- [4] X.M. Bai, B. Shah, L.M. Keer, Q.J. Wang, and R.Q. Snurr. Particle dynamics simulations of a piston-based particle damper. *Powder Technol.*, 189:115, 2009.
- [5] X.M. Bai, L.M. Keer, Q.J. Wang, and R.Q. Snurr. Investigation of particle damping mechanism via particle dynamics simulations. *Granular Matter*, 11:417, 2009.
- [6] M.N. Bannerman, J.E. Kollmer, A. Sack, M. Heckel, P. Mueller, and T. Pöschel. Movers and shakers: Granular damping in microgravity. *Physical Review E*, 84: 011301, 2011.
- [7] M. Heckel, A. Sack, J.E. Kollmer, and T. Pöschel. Granular dampers for the reduction of vibrations of an oscillatory saw. *Physica A*, 391:4442–4447, 2012.
- [8] D.I. Ryzhkov. Vibration damper for metal cutting. *The Engineer's Digest*, 14:246, 1953.
- [9] S. Ashley. A new racket shakes up tennis. *Mechanical Engineering*, 117:80–81, 1995.
- [10] K.W. Chan, W.H. Liao, M.Y. Wang, and P.K. Choy. Experimental studies for particle damping on a bond arm. *J. Vib. Control*, 12:297–312, 2006.
- [11] Z. Xia, X. Liu, and Y. Shan. Application of particle damping for vibration attenuation in brake drum. *Int.J.Veh.Noise Vib.*, 7:178–194, 2011.
- [12] H.V. Panossian. Structural damping enhancement via non-obstructive particle damping technique. *Journal of Vibration and Acoustics*, 114(1):101–105, 1992.

- [13] Clara Salueña, T. Pöschel, and S.E. Esipov. Dissipative properties of vibrated granular materials. *Physical Review E*, 59(4):4422, 1999.
- [14] A. Sack, M. Heckel, J.E. Kollmer, F. Zimber, and T. Pöschel. Energy dissipation in driven granular matter in the absence of gravity. *Physical Review Letters*, 111: 018001, 2013.
- [15] J.E. Kollmer, A. Sack, M. Heckel, and T. Pöschel. Relaxation of a spring with an attached granular damper. *New Journal of Physics*, 15:093023, 2013.
- [16] A. Sack, M. Heckel, J.E. Kollmer, and T. Pöschel. Probing the validity of an effective-one-particle description of granular dampers in microgravity. *Granular Matter*, 17:73, 2015.
- [17] H.M. Jaeger and S.R. Nagel. Physics of the granular state. *Science*, 255:1523, 1992.
- [18] K.M. Mao, M.Y. Wang, Z.W. Xu, and T.N. Chen. Simulation and charaterization of particle damping in transient vibrations. *J.Vib.Acoust.*, 126:202, 2004.
- [19] X. Fang and J. Tang. Granular damping in forced vibration qualitative and quantitative analysis. *J.Vib.Acoust.*, 128:489, 2006.
- [20] R.D Nayeri, S.F. Masri, and J.P. caffrey. Studies of the performance of multi-unit impact dampers under stochastic excitation. *J.Vib.Acoust.*, 129:239, 2007.
- [21] T. Pöschel and T. Schwager. *Computational Geanular Dynamics*. Springer, 2004.
- [22] H. Hinrichsen and D.E. Wolf, editors. *The Physics of Granular Media*. WILEY-VCH, 2004.
- [23] H. Kruggel-Emden, E. Simsek, S. Rickelt, S. Wirtz, and V. Scherer. Review and extension of normal force models for the discrete element model. *Powder Twchnology*, IV, 2007.
- [24] J. Schäfer, S. Dippel, and D.E. Wolf. Force schemes in simulations of granular materials. *J.Phys. I France*, 6:5, 1996.
- [25] K.L. Johnson. *Contact Mechanics*. Cambridge university press, 1985.
- [26] N.V. Brilliantov, F. Spahn, J.M. Hertzsch, and T. Pöschel. Model for collisions in granular gases. *Phys. Rev. E*, 1996.
- [27] T. Schwager and T. Pöschel. Coefficient of restitution for viscoelastic spheres: The effect of delayed recovery. *Phys. Rev. E*, 78:051304, 2008.

- [28] P. Müller and T. Pöschel. Collision of viscoelastic spheres:compact expressions for the coefficient of normal restitution. *Phys. Rev. E*, 84:021302, 2011.
- [29] H.P. Zhang and H.A. Makse. Jamming transition in emulsion and granular materials. *Physical Review E*, 72:011301, 2005.
- [30] C. Kloss, C. Goniva, A. Hager, S. Amberger, and S. Pirker. Models, algorithms and validation for opensource dem and cfd-dem. *Prog. Comput. Fluid Dyn.*, 12, 2012.
- [31] E.J.R. Parteli, J. Schmidt, C. Blümel, K.E. Wirth, W. Peukert, and T. Pösche. Attractive particle interaction forces and packing density of fine glass powders. *Nature - Scientific Reports*, 4:6227, 2014.
- [32] C. H. Rycroft, A.V. Orpe, and A. Kudrolli. Physical test of a particle simulation model in a sheared granular system. *Phys. Rev. E*, 80:031035, 2009.
- [33] M. Griebel, S. Knapek, and G. Zumbusch, editors. *Numerical Simulation in Molecular Dynamics*. Springer, 2007.
- [34] D. Queteschiner and C. Kloss. Introduction to dynamical particle simulations.
URL <http://www.www.cfdem.com>.
- [35] P. Müller, D. Krengel, and T. Pöschel. Negative coefficient of normal restitution. *Phys. Rev. E*, 85:041306, 2012.
- [36] S. Luding. Introduction to discrete element methods. *EJECE*, 12:785, 2008.
- [37] S. McNamara and W.R. Young. Inelastic collapse and dumping in a one-dimensional granular medium. *Phys. Fluids A*, 4(3), 1992.
- [38] K.S. Marhadi and V.K. Kinra. Particle impact damping: effect of mass ratio,material, and shape. *J.Sou.Vib*, 283:433, 2005.
- [39] R.K. McGeary. Mechanical packing of spherical particles. *Journal of The american Ceramic society*, 44(10), 1962.
- [40] J.G. Berryman. Random close packing of hard spheres and disks. *Phisycal Review A*, 27(2):1053, 1983.
- [41] C. Song, P. Wang, and H.A. Makse. A phase diagram for jammed matter. *Nature*, 453(7195):629, 2008.
- [42] M. Sánchez, G. Rosenthal, and L.A. Pugnaloni. Universal response of optimal granular damping devices. *Journal of Vibration and Control*, 331(20):4389, 2012.

- [43] T.A. Jadhav and P.J. Awasare. Enhancement of particle damping effectiveness using multiple cell enclosure. *Journal of vibration and control*, 2014.
- [44] M. Saeki. Analytical study of multi-particle damping. *Journal of sound and vibration*, 281:1133, 2005.
- [45] C.X. Wong, A.B. Spencer, and J.A. Rongong. Effect of enclosure geometry on particle damping performance. *50th AIAA/ASME/ASCE/AHS/ASC Structures, Structural Dynamics, and Materials Conference*, 4 - 7 May 2009, Palm Springs, California.
- [46] F. Pacheco-Vazquez and S. Dorbolo. Rebound of a confined granular material: combination of a bouncing ball and a granular damper. *nature*, (2158), 2013.